
UNIVERSIDAD POLITÉCNICA DE VALENCIA

Máster en electrónica e informática industrial

# Control of constrained biosystems

Ana Revert Tomás

Supervisor: Jesús Picó i Marco

Supervisor: Jorge Bondia Company

April 2011

This work is partially supported by the Spanish Government under grants DPI-2007-66728, DPI-2010-20764-C02 and DPI-2008-06880-C03-01. The author is also recipient of a fellowship from the Spanish Ministry of Science and Innovation (FPI BES-2009-020327).

# Contents

# List of Tables

# List of Figures

# Rationale and objetives of the Master Thesis

Biological and biomedical systems (biosystems) are becoming one of the challenging research topics in the field of systems and control. Those systems are complex systems with the main characteristics of them, that is, high state-space dimension, multiple inputs and outputs, external disturbances, significant non-linearity and uncertainty...

Apart from their scientific interest, biosystems attractiveness lies also in their multidisciplinary character and their relation with life sciences.

Biomedical systems involve a multitude of interacting subsystems and networks, with multiple feedforward and feedback loops, and interactions at many levels. The dynamics vary from one individual to another, and within the same individual over time. Usually internal states can not be measured, and are difficult to estimate.

In a similar way, biological systems and metabolic networks, also offer interesting properties for control. Usually the variables that want to be controlled can not be measured and have to be estimated. This estimation has to be carried out taking into account uncertainty and the low ratio

between measured variables versus model variables. The recent availability of experimentally validated models has impulsed definitively the analysis and control of this kind of problems.

Constraints and non-linearities are often present in biosystems. Sometimes the internal variables of the processes have bounded ranges of operation. And, in other occasions theses restrictions are imposed in order to improve the performance of the system. They can be applied in the output, to keep it between two values or below/above one limit, or to internal states or combinations of states.

It is important not to forget the academic motivation of this work. Indeed, the master thesis presentation is the last necessary step to obtain the Master's Degree In Automation And Industrial Computing.

The main **objective** of this thesis is:

*"To study different strategies to deal with control of processes subject to constraints in the context of biomedical and biological systems".*

The methodologies used to carry out this main objective, together with its chapter distribution, is shown in figure 1.

In a **first phase** a study of the possible tools to deal with problems when constraints are present in one or another way was carried out. As a result, chapter 1 explains the main theoretical concepts of the tools that are used in this work. In that way, interval techniques to deal with constraints under uncertainty, and the specific features of sliding modes when used to solve control problems where constraints exist or are imposed in some state or combinations of states, are exposed in detail.

The **second phase** consisted in adapting and applying those tools to different "bio-problems". On one hand, chapter 2 deals with the complicated

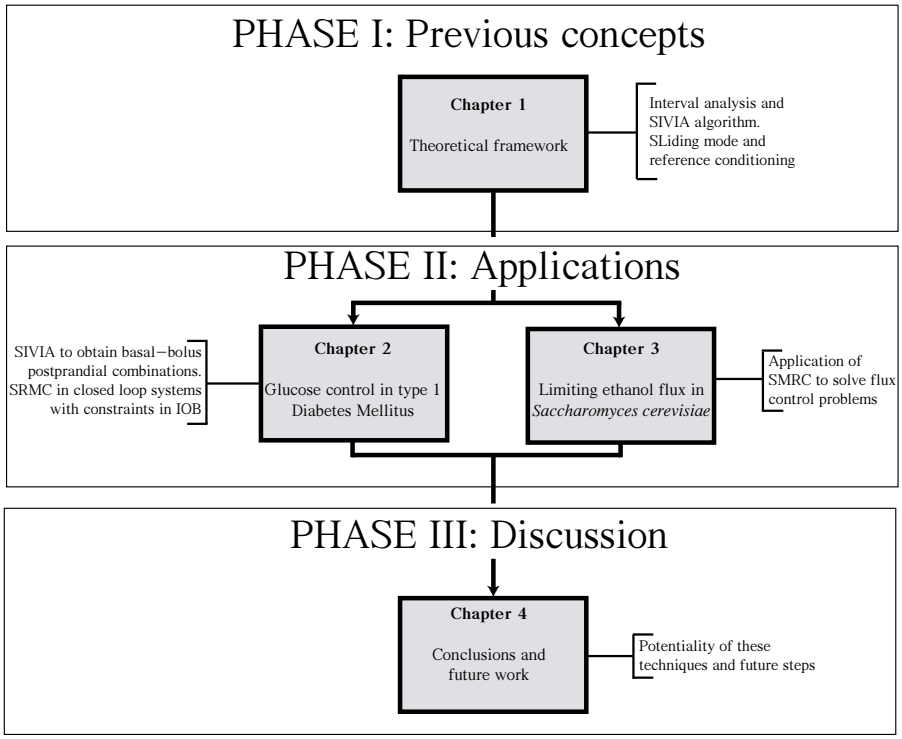


Figure 1: Methodology and thesis structure

problem of glucose control in type 1 diabetes mellitus, proposing two strategies to improve postprandial control. And, on the other hand, chapter 3 introduces the problem of internal fluxes control in metabolic networks.

Finally, the **third phase**, which in fact was developed in parallel with the rest of the phases, was focused on the search of opportunities to extend the tools used here. The objective is to solve more interesting and realistic problems in bio-systems, where uncertainty and lack of measures is the common denominator. These conclusions and future work possibilities can be found in chapter 4.

Chapter 1

# Theoretical framework

## 1.1 Introduction

In this chapter, the main theoretical concepts that will be used in the following chapters are explained in detail. On one hand, concepts of interval analysis, particularly suitable to deal with constraints under uncertainty, and their application to solve set inversion problems (SIVIA) are provided (section 1.2). On the other hand, the basis of sliding mode reference conditioning (SMRC) techniques are explained thoroughly in section 1.3.

## 1.2 Interval Analysis and Set Inversion

Interval analysis arose in the context of numerical analysis and the study of propagation of computational errors in finite number systems [56, 65]: if real numbers are substituted by compact subsets of the digital scale (intervals) which contain it, and real operators by interval operators, computations will lead to intervals that contain the actual solution, whose width is a measure of the approximation error. It is precisely this property of inclusion of the actual

solution that makes interval analysis and methods derived very interesting when a *mathematical guarantee* is desired.

Inclusion functions are thus one of the fundamental tools in interval analysis.

In the following, during this section and section 2.4, $[x]$ will denote a real interval, and $\underline{x}$, $\overline{x}$ are its left and right endpoints. Interval vectors, or boxes, will be denoted in boldface, $[\mathbf{x}]$. The set of all real intervals will be denoted by $\mathbb{IR}$ and the set of $n$-dimensional boxes as $\mathbb{IR}^n$.

A formal definition follows.

**Definition 1.2.1** *Given a function* $\mathbf{f} : \mathbb{R}^n \to \mathbb{R}^m$*, the interval function* $[\mathbf{f}] : \mathbb{IR}^n \to \mathbb{IR}^m$ *is an inclusion function for* $\mathbf{f}$ *if for any box* $[\mathbf{x}] = [\underline{\mathbf{x}}, \overline{\mathbf{x}}] \in \mathbb{IR}^n$

$$[\mathbf{f}]([\mathbf{x}]) \supseteq [\min_{\mathbf{x}\in[\mathbf{x}]} \mathbf{f}(\mathbf{x}), \max_{\mathbf{x}\in[\mathbf{x}]} \mathbf{f}(\mathbf{x})].$$

The simplest way to get an inclusion function for $\mathbf{f}$ is replacing the real variable $x$ with an interval variable $[x]$ and the real arithmetic operations with corresponding interval operations. The result $[\mathbf{f}]$ is called a *natural inclusion function* of $\mathbf{f}$[56]. However, this may yield significant overestimation when multiple instances of a variable appear in the expression to evaluate (multiincidences problem). Other inclusion functions have been studied to reduce this problem like centered forms or Taylor expansion forms. See for instance [2, 65, 56, 38] for more details on this topic.

Currently, interval analysis is a mature technology that has been successfully applied in fields aside numerical analysis such as robotics, control, computer graphics, economy, global optimization, and fault detection, among others [38].

An important application of interval analysis is the solution of set inversion problems. Let $\mathbb{X} \subseteq \mathbb{R}^n$ and $\mathbb{Y} \subseteq \mathbb{R}^m$ be an input and output

space, respectively. Given a set $\mathcal{Y} \subseteq \mathbb{Y}$ and a map $\mathbf{f} : \mathbb{X} \to \mathbb{Y}$, the set $\mathcal{X} := \{\mathbf{x} \in \mathbb{X} \mid \mathbf{f}(\mathbf{x}) \in \mathcal{Y}\}$ is sought. The set $\mathcal{Y}$ is usually defined through constraints on the output space. The SIVIA algorithm [38] makes use of a branch-and-bound technique together with interval analysis to get an approximation of the solution set $\mathcal{X}$. This approximation is done in terms of subpavings (collection of boxes of the appropriate dimension with non-overlapping interiors). An inner and outer subpaving, which will be denoted as $[\mathcal{X}]_{\mathrm{i}}$ and $[\mathcal{X}]_{\mathrm{o}}$ respectively, are built so that $[\mathcal{X}]_{\mathrm{i}} \subseteq \mathcal{X} \subseteq [\mathcal{X}]_{\mathrm{o}}$. Hence, it is guaranteed that $[\mathcal{X}]_{\mathrm{i}}$ will contain only solutions while the complementary set of $[\mathcal{X}]_{\mathrm{o}}$, denoted as $\overline{[\mathcal{X}]_{\mathrm{o}}}$, will contain only non-solutions (see figure 1.1).

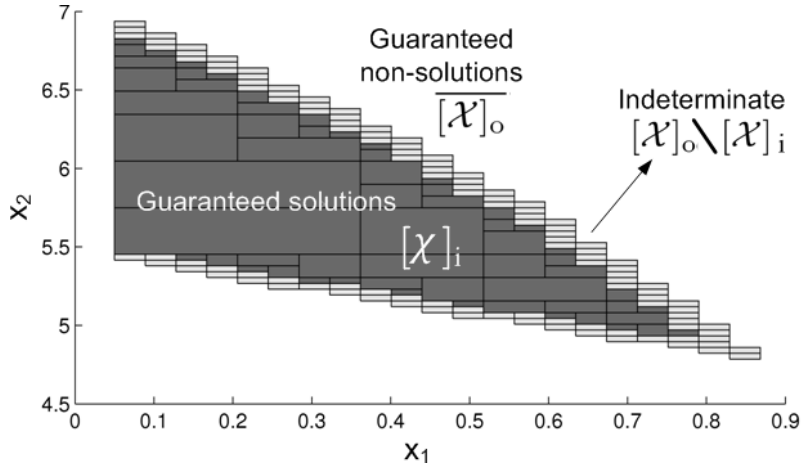


Figure 1.1: Plot that illustrates the concept of inner and outer subpaving. The dark rectangles represent the inner subpaving and guarantee the fulfillment of the constraints. The outer subpaving is made up of both the dark and the light rectangles. Its complementary set (in white) is guaranteed to contain only *non-solutions* that violate some of the constraints. Results in the boundary (light rectangles) are unknown a priori.

Some previous definitions follow before presenting the SIVIA algorithm.

**Definition 1.2.2** *The width of a box* $[\mathbf{x}] = [\underline{\mathbf{x}}, \overline{\mathbf{x}}] \in \mathbb{IR}^n$ *is* $w([\mathbf{x}]) := \max_{i \in \{1,\ldots,n\}} (\overline{x_i} - \underline{x_i})$.

**Definition 1.2.3** *The midpoint of a box* $[\mathbf{x}] = [\underline{\mathbf{x}}, \overline{\mathbf{x}}] \in \mathbb{IR}^n$ *is* $m([\mathbf{x}]) := (\underline{\mathbf{x}} + \overline{\mathbf{x}})/2$.

**Definition 1.2.4** *The left and right children of a box* $[\mathbf{x}] = [\underline{\mathbf{x}}, \overline{\mathbf{x}}] \in \mathbb{IR}^n$ *are*

$$L([\mathbf{x}]) := [\underline{x_1}, \overline{x_1}] \times \cdots \times [\underline{x_j}, m([x_j])] \times \cdots \times [\underline{x_n}, \overline{x_n}]$$
$$R([\mathbf{x}]) := [\underline{x_1}, \overline{x_1}] \times \cdots \times [m([x_j]), \overline{x_j}] \times \cdots \times [\underline{x_n}, \overline{x_n}]$$

*where* $j$ *is the first component of* $[\mathbf{x}]$ *with maximum width, that is,* $j = \min\{i \mid w([x_i]) = w([\mathbf{x}])\}$.

**Algorithm 1.2.1** *[SIVIA, [38]]*

*Let* $\mathcal{X}$ *be the solution set sought and* $[\mathcal{X}]_{\mathrm{i}}$ *and* $[\mathcal{X}]_{\mathrm{o}}$ *be two subpavings corresponding to inner and outer approximations of* $\mathcal{X}$ *as defined above. Let* $[t] : \mathbb{IR}^n \to \mathbb{IB}$ *be a test interval function from the set of n-dimensional interval vectors (box in the input space) to the set of interval booleans,* $\mathbb{IB} = \{0, 1, [0, 1]\}$ *(where* 0 *stands for false,* 1 *for true and* $[0, 1]$ *for indeterminate). Finally, let* $[\mathbf{x}] \in \mathbb{IR}^n$ *be an initial box in the input space and* $\epsilon$ *be a positive precision factor that can be chosen arbitrarily low. The SIVIA algorithm is as follows:*

| *SIVIA(in:* $[t]$,$[\mathbf{x}]$,$\epsilon$, *out:* $[\mathcal{X}]_{\mathrm{i}}$,$[\mathcal{X}]_{\mathrm{o}}$*)* |
|---|
| *if* $[t]([\mathbf{x}]) = 0$, *return;* |
| *if* $[t]([\mathbf{x}]) = 1$, |
| *then* $\{[\mathcal{X}]_{\mathrm{i}} := [\mathcal{X}]_{\mathrm{i}} \cup [\mathbf{x}]$; $[\mathcal{X}]_{\mathrm{o}} := [\mathcal{X}]_{\mathrm{o}} \cup [\mathbf{x}]$; *return;* $\}$; |
| *if* $w([\mathbf{x}]) < \epsilon$, |
| *then* $\{[\mathcal{X}]_{\mathrm{o}} := [\mathcal{X}]_{\mathrm{o}} \cup [\mathbf{x}]$; *return;*$\}$; |
| *SIVIA(*$[t]$,$L([\mathbf{x}])$,$\epsilon$,$[\mathcal{X}]_{\mathrm{i}}$,$[\mathcal{X}]_{\mathrm{o}}$*);* |
| *SIVIA(*$[t]$,$R([\mathbf{x}])$,$\epsilon$,$[\mathcal{X}]_{\mathrm{i}}$,$[\mathcal{X}]_{\mathrm{o}}$*);* |

The inner subpaving will thus consist of the boxes classified as *true*, while the outer subpaving contains the *true* and *indeterminate* boxes (of width smaller than the tolerance defined). Not small enough *indeterminate* boxes will be splitted in two subboxes by the midpoint of its largest dimension and the procedure repeated.

## 1.3 Sliding mode

A variable structure system (VSS) is composed by two or more subsystems and a logic which decides when the switching between those systems will take place. The resulting control law is a discontinuous function of the states of the system. When the switching frequency is elevated, a very interesting operation mode is obtained: the states of the system are constrained to a manifold in the state space. This particular operation mode is named sliding mode (SM), and it presents very attractive features.

In the end of the 70's the interest in VSS started to grow and, since then, great theoretical advances have been carried out in the field. Several general revisions of VVS can be found in literature [79, 33, 17, 80, 90, 61, 16]. Moreover, the interesting properties of the SM and the last technological development has allowed the implementation of many practical applications of SM algorithms [27, 11, 42, 34].

The SM control principles will be explained in this section, following the general lines of [71, 72]. Finally, the algorithm that is going to be used in part of this work which is based in those principles is presented.

### 1.3.1 Description of the sliding mode

Consider the following non-linear dynamical system:

$$\begin{cases} \dfrac{dx}{dt} = f(x) + g(x)u, \\ y(t) = h(x), \end{cases} \tag{1.1}$$

where $x \in \mathbf{X} \subset \mathbb{R}^n$ is the system state, $u \in \mathbb{R}$ the control signal (possibly discontinuous), $f : \mathbb{R}^n \longrightarrow \mathbb{R}^n$ and $g : \mathbb{R}^n \longrightarrow \mathbb{R}^n$ two vectorial fields in $\mathcal{C}^n$ (many times differentiable) and $h(x) : \mathbb{R}^n \longrightarrow \mathbb{R}$ a scalar field also in $\mathcal{C}^n$, all

defined in $\mathbf{X}$, with $g(x) \neq 0$, $\forall x \in \mathbf{X}$. This kind of systems are named affine in control systems.

Define $s(x)$ as a smooth function on $\mathbf{X}$ like $s : \mathbf{X} \longrightarrow \mathbb{R}$, with $\nabla s \neq 0, \forall x \in \mathbf{X}$. Then the set

$$\mathcal{S} = \{x \in \mathbf{X} : s(x) = 0\}, \tag{1.2}$$

defines a locally regular manifold of $(n-1)$ dimension on $\mathbf{X}$, named *sliding manifold* or *switching surface*.

A variable structure control law can be defined to enforce the control action $u$ to take one of two different values according to the sign of the switching function $s(x)$ (often addressed as an auxiliary output),

$$u = \begin{cases} u^+(x) & if \quad s(x) > 0 \\ u^-(x) & if \quad s(x) < 0 \end{cases} \qquad u^-(x) \neq u^+(x) \tag{1.3}$$

where the upper and lower values of $u$ are smooth functions of $x$ and, without loss of generality, they are assumed to satisfy $u^-(x) < u^+(x)$ and $u^-(x) \neq u^+(x)$ locally in $\mathbf{X}$.

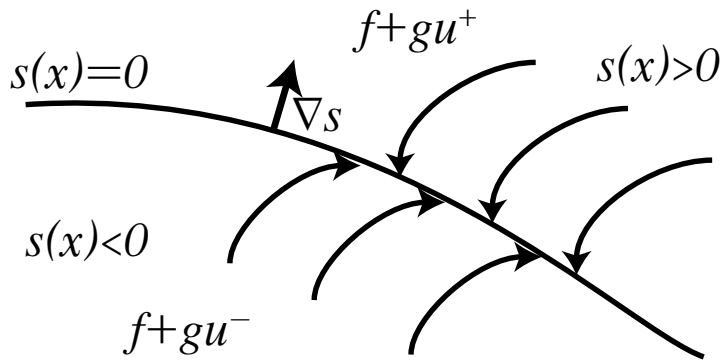


Figure 1.2: Sliding regime on the switching manifold $s(x) = 0$

Then, a sliding mode will exist on $\mathcal{S}$ as a result of the switching law

(1.3), when the system reaches the manifold $\mathcal{S}$ and stays locally in its neighbourhood. For a sliding regime to exist on $\mathcal{S}$, both controlled vector fields of each continuous subsystem, $(f + gu^+)$ and $(f + gu^-)$, should point locally towards the manifold $\mathcal{S}$.

The geometrical representation of the previous situation is depicted in figure 1.2.

**Sliding mode existence necessary condition**

It has been mentioned before that, in order to ensure that a sliding mode sets up in the surface $s(x) = 0$, both controlled vector fields switched by 1.3 should point towards the manifold $\mathcal{S}$. This implies mathematically that:

If the next inequalities hold for the switching function, locally on $\mathcal{S}$ as a result of the control action (1.3):

$$\begin{cases} \dot{s}(x) < 0 & if \quad s(x) > 0 \\ \dot{s}(x) > 0 & if \quad s(x) < 0 \end{cases} \tag{1.4}$$

then the state trajectories of the system (1.1) locally reach the sliding manifold $\mathcal{S}$ and, from there on, their motion is constrained to immediate vicinity of $\mathcal{S}$.

To take advantage of the natural geometric interpretation of some sliding mode related concepts, in the following Lie derivative will be used:

$$L_f h(x) : \mathbb{R}^n \longrightarrow \mathbb{R}$$

that is, the derivative of the scalar field $h(x) : \mathbb{R}^n \longrightarrow \mathbb{R}$ in the direction of the vectorial field $f(x) : \mathbb{R}^n \longrightarrow \mathbb{R}^n$:

$$L_f h(x) = \frac{dh}{dx} f$$

Like every derivative, *Lie derivative* is a linear operator. Then taking derivative of the switching function $s(x)$ one gets

$$\dot{s}(x) = L_{f+gu} s(x) = L_f s(x) + L_g s(x) u \tag{1.5}$$

The using the last differential geometry tools, equation (1.4) can be rewritten using the first equality of (1.5),

$$\begin{cases} \lim\limits_{s(x)\to 0^+} L_{f+gu^+} s(x) < 0 \\ \lim\limits_{s(x)\to 0^-} L_{f+gu^-} s(x) > 0 \end{cases} \tag{1.6}$$

This last equation implies the rate of change of the scalar surface coordinate function $s(x)$, measured in the direction of the controlled field, is such that a crossing of the surface is guaranteed, from each side of the surface, by use of the switching policy (1.3). The same can be written in a more compact form:

$$\lim_{s(x)\to 0} s(x) \cdot \dot{s}(x) < 0. \tag{1.7}$$

Then thanks of the linearity properties of the *Lie derivative*, equation (1.5) can be expressed in a equivalent way:

$$\begin{cases} L_f s + L_g s u^+ < 0 \quad if \quad s > 0 \\ L_f s + L_g s u^- > 0 \quad if \quad s < 0 \end{cases} \tag{1.8}$$

*Note:* From now on, we will drop parenthesis unless we want to expressly show some function dependance from a particular variable.

So in order to establish the sliding mode on $s(x) = 0$ the following should

be satisfied

$$L_g s = \frac{\partial s}{\partial x} g \neq 0 \tag{1.9}$$

locally in $\mathcal{S}$. The previous condition is a necessary reaching condition for sliding mode, and is known as *transversality condition*.

**Remark 1.3.1** *Supposing, without loss of generality, that $u^-(x) < u^+(x)$ is satisfied, then the necessary existence condition of a slinging regime over $\mathcal{S}$ is given by*

$$L_g s = \frac{\partial s}{\partial x} g < 0 \tag{1.10}$$

*locally in a vicinity of $\mathcal{S}$.*

*The demonstration is immediate from* (1.8)*: subtracting both expressions for $\dot{s}$ it must hold*

$$\left(u^+(x) - u^-(x)\right) L_g s < 0$$

*And as it was $u^+(x) - u^-(x) > 0$, the condition becomes $L_g s < 0$.*

As a particular case, we will analyze some properties of the sliding mode control in linear systems with the structure described in figure 1.3. In this particular case the system description is

$$\begin{aligned} \dot{x} &= Ax + bu, \\ y &= c^T x, \end{aligned} \tag{1.11}$$

where the control action $u$ is determined by (1.3). Then the functions defined for the systems (1.1) are in the system (1.11) given by

$$f(x) = Ax, \tag{1.12}$$

$$g(x) = b, \tag{1.13}$$

$$h(x) = c^T x. \tag{1.14}$$

Consider the following switching law:

$$s(x) = k^T x - k_r r \tag{1.15}$$

where the constant $k_r$ must be choose in such way the value of the steady state output will be equal to the set-point r and the constants $k^T$ will determine the linear dynamics when the system is working in sliding mode.

The trajectories of the states should point to wardsthe surface $s(x) = 0$ from both sides. So, when $s(x) > 0$, $s(x)$ should decrease. The same in the inverse sense. This is guaranteed by the transversality condition, which according to (1.13) and (1.15) here is given by

$$L_g s = \frac{\partial s}{\partial x} g = k^T b \neq 0 \tag{1.16}$$

So for the system (1.11) and the switching function (1.15) it results

$$\dot{s}(x) < 0 \quad \Rightarrow \dot{s}(x, u^+) \quad = k^T A x + k^T b u^+ < 0 \tag{1.17}$$

$$\dot{s}(x) > 0 \quad \Rightarrow \dot{s}(x, u^-) \quad = k^T A x + k^T b u^- > 0 \tag{1.18}$$

In both inequalities, the first two terms are equal at both sides of the switching surface, then the las term is the only one which can change the sign of the expression.

Now, considering the set-point $r = 0$, the transfer function between discontinuous action and the switching surface is given by:

$$\frac{S}{U} = -k^T \left(sI - A\right)^{-1} b. \tag{1.19}$$

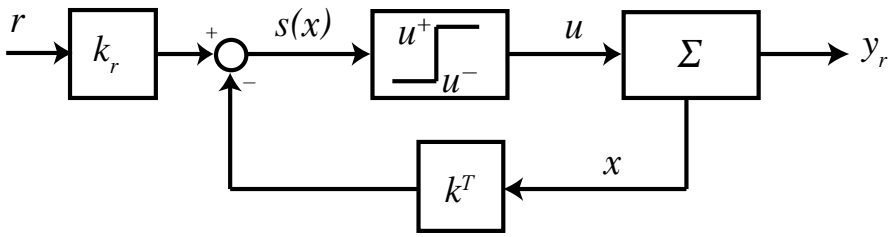


Figure 1.3: Conventional scheme of sliding mode control.

Which can be developed into its Taylor series:

$$\frac{S}{U} = (-k^T)bs^{-1} + (-k^T)Abs^{-2} + (-k^T)A^m bs^{-(m+1)} + \dots \tag{1.20}$$

So, the transversality condition imposes the first term of Taylor decomposition ($k^T b$ is also the first Markov parameter of the system) has to be different from zero. This can be translated in the following condition:

*The transfer function between the discontinuous action and the switching surface must have unitary relative degree [72].*

Anyway, the transversality condition is only a necessary condition, but not a sufficient one to guarantee the existence of the sliding mode.

**Equivalent control method**

The system in a sliding regime, ideally implies infinite frequency switching, *i.e.*, is discontinuous at every time instant. This precludes obtaining an analytical solution of the state equation. One way to obtain the sliding mode dynamics consist in finding a continuous system equivalent to the sliding mode.

To this end, the *ideal sliding mode* is the regime of ideal operation in which the manifold $\mathcal{S}$ is an invariant manifold of the system. In this conditions, once the system trajectories reach the manifold, they slide exactly on the manifold and never leave it.

The invariance condition of the manifold $\mathcal{S}$ is given by:

$$\begin{cases} s(x) = 0 \\ \dot{s}(x) = L_f s(x) + L_g s(x) u_{eq} = 0 \end{cases} \tag{1.21}$$

The second equation of (1.21) indicates the trajectories will remain on the surface, meanwhile $u_{eq}(x)$ represents a smooth control law for which $\mathcal{S}$ is an invariant manifold of the system. Then the control $u_{eq}(x)$ is known as *equivalent control* and it can be cleared from (1.21), resulting:

$$u_{eq}(x) = -\frac{L_f s(x)}{L_g s(x)} \tag{1.22}$$

In equation (1.22) is possible to see the transversality condition (1.9) is a necessary and sufficient condition for the well definition of the equivalent control. For the system (1.11) and the switching surface (1.15), the invariance condition is given by:

$$s(x) \quad = k^T x - k_r r = 0 \tag{1.23}$$

$$\dot{s}(x) \quad = k^T \left( Ax - b u_{eq} \right) = 0 \tag{1.24}$$

From equations (1.22) and (1.24) is possible to obtain

$$u_{eq}(x) = -\frac{L_f s(x)}{L_g s(x)} = -\left( \frac{\partial s}{\partial x} b \right)^{-1} \frac{\partial s}{\partial x} Ax = -\left( k^T b \right)^{-1} k_T A x \tag{1.25}$$

Here again, its possible to see transversality condition $\left( k^T b \neq 0 \right)$ should hold so the equivalent control of the sliding mode is well defined.

**A necessary and sufficient condition for existence of Sliding Mode**

By definition, the equivalent control action, is the necessary continuous

control to make the trajectories of the system remain in the invariant manifold. As a consequence, the derivative of the switching function, should also be zero along that trajectory:

$$\dot{s}(x) = L_f s + L_g s u_{eq} = 0 \tag{1.26}$$

which was established in the invariance condition (1.21) of the manifold $\mathcal{S}$.

The next theorem, demonstrated in [71], defines a necessary and sufficient condition for the existence of a sliding mode, in terms of the equivalent control $u_{eq}$.

**Theorem 1.3.1** *Let $u^-(x) < u^+(x)$ and $L_g s < 0$, a necessary and sufficient condition for the local existence of a sliding regime on $\mathcal{S}$, that is locally in $\mathbf{X}$ fox $x \in \mathcal{S}$,*

$$u^-(x) < u_{eq}(x) < u^+(x) \tag{1.27}$$

*In other words, the equivalent control $u_{eq}(x)$ is a kind of average between the lower and upper bounds of the control action. The discontinuous control action can be interpreted as the sum of a low frequency component ($u_{eq}(x)$) and a high frequency one which is filtered out by the system.*

**Ideal sliding mode dynamics** From the expression of the equivalent control, found in (1.22), it follows that the dynamics on $\mathcal{S}$, due to the equivalent control, are governed by

$$\dot{x} = f + g u_{eq}(x) = \left[ I - g \left( \frac{\partial s}{\partial x} g \right)^{-1} \frac{\partial s}{\partial x} \right] f = F(x) f(x) \tag{1.28}$$

Equation (1.28) represents an idealized version of the dynamics in the sliding manifold $\mathcal{S}$ and they constitute an average description for the behaviour of the controlled trajectories of (1.1) and (1.1) on the sliding manifold $\mathcal{S}$. Its easy to notice that the manifold invariance condition (1.21) implies that

$$F(x) f(x) \in \ker(\nabla s). \tag{1.29}$$

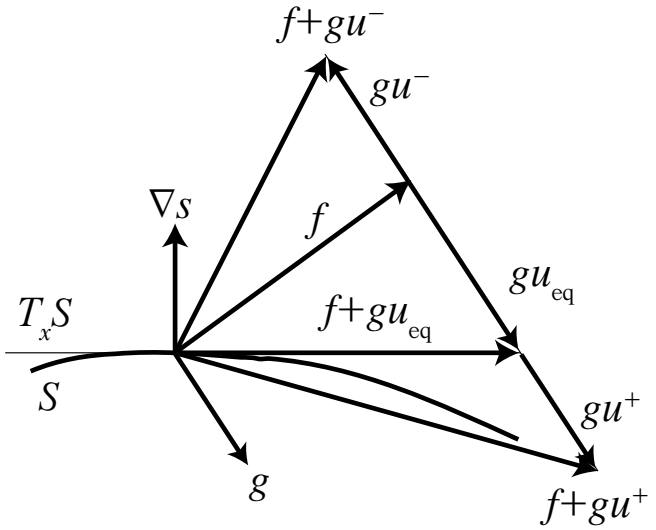


Figure 1.4: Ideal sliding dynamics. Geometric Interpretation of the operator $F$ .

Which means that $F(x)$ can be considered as a projection operator that applies on the vector $f(x)$ and projects it into the tangent plane of $\mathcal{S}$ in $x$. Then, considering a vector $v(x)$ collinear with $g(x)$, *i.e.*$v \in span(g)$

$$v(x) = g(x)\mu(x), \quad \text{with} \quad \mu(x) \in \mathbb{R} \tag{1.30}$$

and applying to this vector $v$ the operator $F(x)$ we obtain

$$F(x)v(x) = \left[ I - g\left(\frac{\partial s}{\partial x} g\right)^{-1} \frac{\partial s}{\partial x} \right] g(x)\mu(x) = 0 \tag{1.31}$$

This means that $F(x)$ annihilates any vector in the direction of $g(x)$, *i.e.* along $span(g)$.

In the figure 1.4 is possible to see that $F(x)f(x)$ is the projection of $f(x)$ onto $\mathcal{S}$ in the direction of $g$, and then the value of $u_{eq}$ is such that $F(x)f(x)$ is tangent to $\mathcal{S}$. This restriction in the state space implies the the system

looses dimension, because it establishes that one state is dependent of the rest of $n-1$ states.

In terms of differential geometry, the following interpretation can be made: The matrix $F(x)$ is a projection operator taking any vector in $\mathrm{T}_x\mathbf{X}$ onto $\Delta_{\mathcal{S}}$ along the $span(g)$, with $\Delta_{\mathcal{S}}$ being the mapping assigning to each $x$, a subspace of the *tangent space* to $\mathbf{X}$ denoted by $T_x\mathbf{X}$ and such that $\langle ds, \Delta_{\mathcal{S}}(x)\rangle = 0$, *i.e.*, $\Delta_{\mathcal{S}}(x) := \ker(ds)$.

The reduced dynamics in the SM can be obtained for the system (1.11). Taking $u_{eq}$ from (1.22) we get

$$\dot{x} = Ax + B\left[-(k^T b)^{-1} k^T A x\right]. \tag{1.32}$$

Then reordering we obtain:

$$\dot{x} = F(x)f(x) = \underbrace{\left(I - b(k^T b)^{-1}k^T\right)A}_{A_{SM}}\, x, \tag{1.33}$$

Is worth to remark that equation (1.33) describes the sliding mode dynamics in a redundant way. One of the state equation is linearly dependent of the other $n-1$ equations. This happens because the state, in the sliding regime, satisfies the restriction $s(x) = 0$, *i.e.* the system trajectories are on the sliding manifold.

The matrix $A_{SM}$ has an eigenvalue at the origin which can be attributed to this redundancy, and does not imply the sliding mode is unstable.

**Remark 1.3.2** *In figure 1.2 is possible to observe the geometric implications of transversality condition* (1.9)*. It establishes the vector field $g(x)$ cannot be tangent to the sliding manifold ($g \ni \ker(\nabla s)$).*

### 1.3.2 Sliding Mode Reference Conditioning

The concept of reference conditioning to achieve a realizable reference, arises in the context of control with restrictions. Specifically, Hanus and Walgama ([24, 84]) applied this kind of solutions to solve the problem of saturation in the actuators (windup). Based on these approaches and getting advance of the possibilities of sliding modes, Mantz and collegues([52, 51, 22]) have applied sliding mode reference conditioning (SMRC) to obtain realizable references under restrictions both in the actuators, in the outputs or in any state or combination of states.

The sliding control loop appears here as an additional loop that makes the reference realizable under certain constraints instead of representing the main control loop. In that way,in contrast with conventional variable structure controllers and sliding modes, the sliding regime is intended as a transitional mode of operation. The conditioning loop is inactive until the system state reaches by itself the sliding surface. It becomes inactive again, when the closed loop system is able to operate again in the non-constrained zone.

It is important to note that, due to the special characteristic of this application, the typical drawbacks of variable structure control and sliding modes (*i.e.* chattering and reaching modes) are avoided.

Let the system

$$\begin{cases} \dfrac{d\mathbf{x}}{dt} = f(\mathbf{x}, p) + g(\mathbf{x})u, \\ \quad y = h_1(\mathbf{x}) \\ \quad v = h_2(\mathbf{x}) \end{cases} \tag{1.34}$$

where $\mathbf{x} \in X \subset \mathbb{R}^n$ is the state vector, $p \in P \subset \mathbb{R}^n$ an unmeasured perturbation, $u \in \mathbb{R}$ is a control input (possibly discontinuous), $f : \mathbb{R}^n \to \mathbb{R}^n$

a vector field, and $h_1(\mathbf{x})$, $h_2(\mathbf{x}) : \mathbb{R}^n \to \mathbb{R}$, scalar fields; all of them defined in $X$.

Variables $y$ and $v$ are both real valued system outputs, $y$ being the main controlled variable, while $v$ is a variable (*e.g.* a measurable state or given function of the states and/or control signal) to be bounded so as to fulfil user-specified system constraints. The bounds on $v$ define the set:

$$\Phi = \left\{ \mathbf{x} \,|\, \phi(v^*) = v - v^+ \leq 0 \right\} \tag{1.35}$$

From a geometrical point of view, the goal is to find a control input $u$ such that the region $\Phi$ becomes invariant (*i.e.* trajectories originating in $\Phi$ remain in $\Phi$ for all times $t$), while $y$ is driven as close as possible to its desired value $r$.

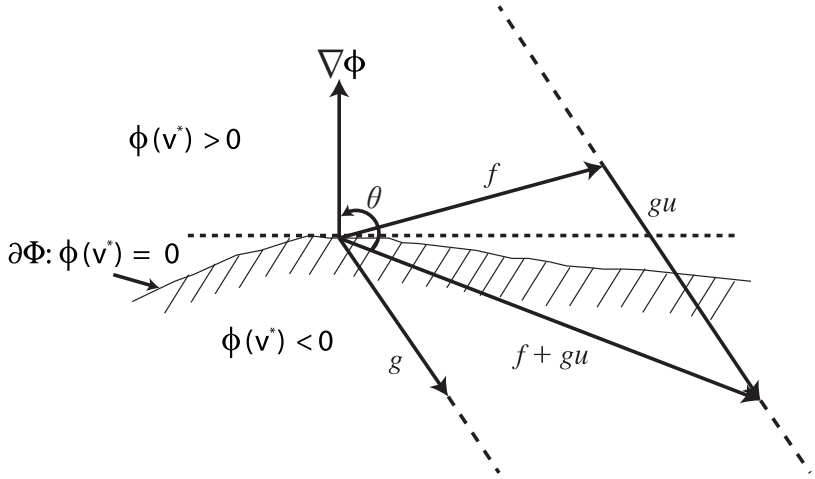


Figure 1.5: Geometric interpretation of invariance conditions

To ensure the invariance of $\Phi$, the control input $u$ must guarantee that the right hand side of the first equation in (1.34) points to the interior of $\Phi$

at all points on the border surface $\partial\Phi = \{\mathbf{x} \mid \phi(v^*) = 0\}$, as shown in figure 1.5.

Mathematically, this condition can be expressed as:

$$\|\nabla\phi\|\|f + gu\| \cos\theta = \nabla\phi^\top \dot{\mathbf{x}} = \dot{\phi}(\mathbf{x}, u) \leq 0, \forall \mathbf{x} \in \partial\Phi \tag{1.36}$$

which constitute, in standard form the *implicit invariance condition* [3, 54]:

$$\sup_u \dot{\phi}(\boldsymbol{x}, u) \leq 0, \textit{ with } \boldsymbol{x} \in \partial\Phi \tag{1.37}$$

Solving 1.37 for $u$, the *explicit invariance control* for system 1.34 is obtained.

In that way,

$$u = (L_g\phi)^{-1}[\dot{\phi} - L_f\phi] = u^\phi + (L_g\phi)^{-1}\dot{\phi} \tag{1.38}$$

with $u^\phi = -L_f\phi / L_g\phi$.

$u$ must be chosen so as to fit equation 1.37.

$$(u - u^\phi) L_g\phi \leq 0, \forall \mathbf{x} \in \partial\Phi \Longrightarrow \tag{1.39}$$

$$u = \begin{cases} \leq u^\phi : \boldsymbol{x} \in \partial\Phi \wedge L_g\phi > 0 \\ \geq u^\phi : \boldsymbol{x} \in \partial\Phi \wedge L_g\phi < 0 \\ \nexists : \boldsymbol{x} \in \partial\Phi \wedge L_g\phi = 0 \\ free : \boldsymbol{x} \in \Phi / \partial\Phi \end{cases} \tag{1.40}$$

with $L_f\phi$ assumed to be possitive.

Note that the transversality condition (equation 1.9) must hold on $\partial\Phi$ for $u^\phi$ to exist. If this is not the case, $\Phi$ should be redefined accordingly.

Also note that once the surface $\Phi$ and the control field g are defined,

only one of the two inequalities will hold. And because of the transversality condition , $L_g\phi$ will remain either positive or negative, but will never change its sign.

**SMRC implementation**

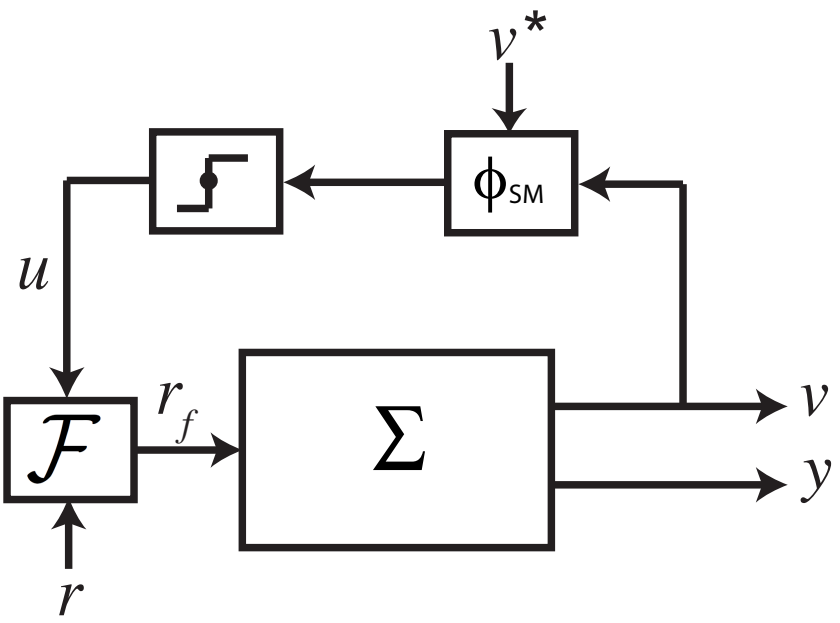


Figure 1.6: SM Reference conditioning general scheme.

Figure 1.6 shows a generic implementation of a reference conditioning loop. It consists of two elements: a filter $\mathcal{F}$ which purpose is to smooth out the conditioned signal $r_f$, and a discontinuous decision block driving the search so as to fulfil the constraints and force the system to remain in the invariance set. Notice that the block $\Sigma$ in the figure may represent a control loop, in which case $r$ is the set-point, and $\mathbf{x}$ in equation (1.34) is the extended state comprising the process, controller, and filter states. The discontinuous decision block is implemented by means of the variable structure control law:

$$u = \begin{cases} u^+ & \text{if} \quad \phi_{SM}(v^*) > 0 \\ 0 & \text{if} \quad \phi_{SM}(v^*) \leq 0 \end{cases} \tag{1.41}$$

where

$$\phi_{SM}(v^*) = v - v^* + \sum_{i=1}^{l-1} \tau_i \, v^{(i)} \tag{1.42}$$

with $l$ being the relative degree between the output $v$ and the input $v$, $v^{(i)}$ the $i$th derivative of $v$, and $\tau_i$ constant gains. The filter $\mathcal{F}$ is implemented as the first-order filter

$$\dot{r}_f = -\alpha \left( r_f + u - r \right), \tag{1.43}$$

with $\alpha$ a design parameter.

Chapter 2

# Glucose control in type 1 Diabetes Mellitus

## 2.1 Introduction

Type 1 diabetes mellitus is a chronic and incurable medical condition that affects millions of people all around the world. It is characterized by a complete lack of insulin production, with the consequence of high blood glucose levels. Since 1921, when insulin was finally isolated for clinical use in humans, and first glucose monitoring techniques were developed, the intensive insulin treatment has undergone important advances.

The Diabetes Control and Complications Trial (DCCT)[15] and the UK Prospective Diabetes Study UKPDS)[78] first demonstrated that chronic hyperglycaemia[1] is responsible for diabetic complications, both in type 1 (T1DM) and type 2 diabetes mellitus (T2DM). A growing body of evidence has stressed the importance of postprandial[2] hyperglycaemia and glycemic variability as possible determinants of diabetes-related complications, as well as increased cardiovascular risk in diabetic people [23, 91]. Indeed,

[1] abnormally high levels of blood glucose concentrations
[2] after-meal

impairment of postprandial control has been shown to be the first alteration of glycaemia homoeostasis contributing to chronic hyperglycaemia [55], and it is associated with an increase of oxidative stress and accelerated atherosclerosis [14, 7].

The need to optimize postprandial control has prompted the development of insulin analogues[3] with more physiologic pharmacokinetic properties [28]. It has also stimulated the research in the field of subcutaneous continuous glucose monitoring (CGM) and continuous subcutaneous insulin infusion (CSII), with the introduction of different bolus strategies and bolus calculators to counteract meal-related blood glucose excursions and to prevent insulin stacking [25, 93]. However, despite the development of these new tools, optimization of postprandial control is still an empiric process, based on both physicians' and patients' experience.

Control of postprandial glycemia excursions is also a barrier to the development of the artificial pancreas[4]. Certainly, meals are one of the major perturbations to counteract and the main challenge found in current clinical validations of the few existing prototypes of automated glycemia control systems [74, 19, 30, 29, 88, 18, 8, 12]. Different approaches have been suggested to deal with meal disturbances in this context, including fully closed-loop systems, semi-closed-loop with meal announcement and hybrid approaches, using Proportional-Integral-Derivative (PID) controllers [74] or algorithms like Model Predictive Control (MPC )[19, 18, 8, 12, 30]. Fully closed-loop systems have shown poor performance, with postprandial glucose higher and post-meal nadir[5] glucose lower than desired [74]. The less-ambitious semi closed-loop and hybrid approaches, have demonstrated improved efficacy as compared with fully closed-loop systems. However,

[3] An altered form of insulin, different from any occurring in nature, but still available to the human body for performing the same action as human insulin in terms of glycemic control.

[4] Technology in development to help people with diabetes automatically control their blood glucose level by providing the substitute endocrine functionality of a healthy pancreas

[5] Lowest point

currently published clinical trials showed unsatisfactory results in terms of postprandial glucose control [8, 12, 30], failing to demonstrate superiority to open-loop control[8, 12]. Indeed, despite the use of meal announcement, the main challenge of currently used control algorithms is still the avoidance of overcorrection and subsequent hypoglycemia[6]. In an attempt to solve this problem, constraints on residual insulin activity (insulin on-board) have been introduced both in PID [74] and MPC-based systems [19] showing an improvement in the incidence of hypoglycemia.

In this chapter, two different approaches are used to try to improve the performance of postprandrial glucose control. Both can be interpreted as solutions to control of processes subject to constraints. First, a constraint satisfaction problem based on the mathematically guaranteed techniques (interval analysis) explained in chapter 1 is posed to calculate the best prandial basal-bolus combination leading to a tight (according to constraints defined by the user) postprandial glucose control. The procedures and results of this work are published in [6, 67, 68]. In the second approach, concepts of SMRC are used to avoid the main problem of current closed loop strategies, the overcorrection and subsequent hypoglycemia. Once a closed loop system is implemented, constraints in the IOB are set so as to reduce that overcorrection, using the same idea as in [74, 19]. The distinguishing feature of this proposal is that it is independent of the controller. That is, it is implemented as an additional control loop that modifies the reference of the main control loop to fulfil the constraints on IOB.

In section 2.2 an introduction of the type of control strategies more used in glucose control and the main problems that can be found is provided. Section 2.3 introduces the types of models used in diabetes and the one that will be used in this work. Section 2.4 is dedicated to the application of interval analysis techniques to obtain tight glucose control. In section 2.5, the details of the application of SMRC to improve the performance of glucose close loop control is provided. Both proposals are validated using the Food and Drug

[6]Blood glucose concentrations abnormally low (bellow 60-70 mg/dL)

Administration (FDA)-accepted University of Virgina (UVa) simulator [37]. Finally, section 2.6 analyzes the potentiality of these techniques and presents future work in this area.

## 2.2 Closed-loop control in type 1 diabetes

Since the 70s, closed loop glucose systems are focussing attention of many researchers. Parallel evolution in the last years both in sensors and insulin delivery devices and in the development of new types of insulins capable of dealing with postprandial glucose excursions (fast-acting analog insulins) has definitely stimulated the development of this kind of systems. In fact, in 2006 the Juvenile Diabetes Research Foundation (JDRF) launched the Artificial Pancreas Project setting up a consortium of Universities and other research organisations to promote collaboration in diabetes research. [7]

The typical control scheme using glucose subcutaneous monitors and insulin external pumps is shown in figure 2.1. Other approaches such as intravenous or intra-peritoneal sensors or insulin infusion systems can be also used, but they are less common than the subcutaneous approaches due mainly to their invasive nature, that makes them less feasible nowadays.

However, some problems arise with this approach. One of the most critical is the input delay caused by the delay of subcutaneous insulin absorption and action, even with fast-acting analog insulin. This problem is specially important after meals, since this delay leads to late and often excessive insulin delivery, leading in turn to hypoglycaemia (overcorrection hypoglycaemia). Stated in engineering terminology, there is an instability characterized by large oscillations in the controlled variable (glucose) due to marked input

[7] Consortium participants include Cambridge University, Boston University, Oregon Health and Science University, Sansum Diabetes Research Institute, Stanford University, University of Colorado, University of Virginia, Yale University, and University of California Santa Barbara.

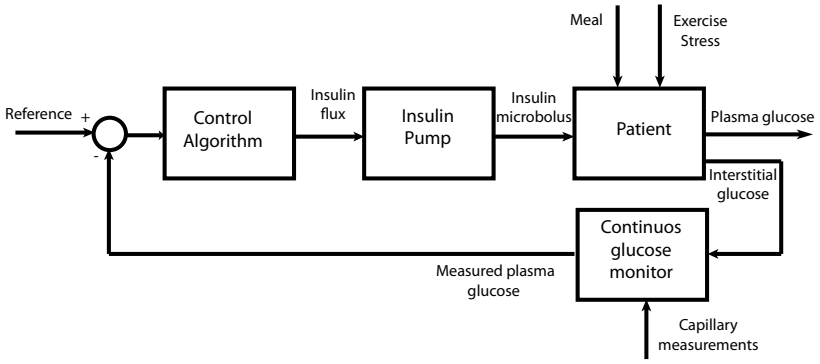


Figure 2.1: Typical glucose closed-loop system

delay. This poor postprandial performance [74] has promoted the use of feed-forward strategies (meal announcement). Patients indicate the time and optionally the carbohydrates (cho) grams of the meal and either a constant or a partial proportional bolus is infused (see figure 2.2). This semi-closed loop or hybrid system involving open-loop insulin delivery before meals has been shown to lead to tighter glycemic control than fully closed loop treatment [88] although they can not eliminate the overcorrection problem.

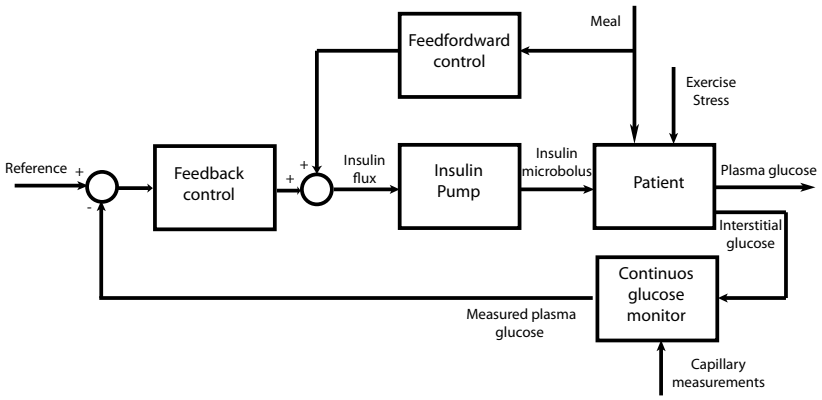


Figure 2.2: Glucose closed-loop system with meal announcement

It must be taken into account that the effect of a meal in the blood glucose depends on many factors, not only on the ingestion time, and the grams of cho. Factors such as the nutritional composition of the meal, the way it has

been cooked and the effect of previous meals makes the meal a no completely measurable perturbation.

Moreover, another important issue that must be considered when thinking in glucose control is variability. This variability is not only referred to inter-patient variability, but also to changes in the insulin sensitivity in the same patient during a day. The insulin sensitivity is subject to circadian variations that affect the insulin requirements for a specific glucose levels [83]. Other sources of intra-patient variability are stress, exercise, infections...

Finally, additional technological problems complicate even more the control. The precision of the glucose subcutaneous sensor is still a challenge due to the presence of relative errors above 20% that, moreover, are often presented as bias errors, inducing again sobreactuation. Problems in the actuator (insulin pumps) arise when they get blocked up or there is a leak.

For all these reasons it is important to note that glucose blood control is a complex problem where finding a solution for all the problems mentioned is a very difficult task. For this reason, partial solutions helping to solve some of the problems mean a big step in the field.

An ideal glucose controller would be one capable of limiting the insulin infusion, minimizing the hypoglycaemia events and robust in the presence of intra-patient variability and errors in the measures. In addition it can not be too complex, and needs to be adjustable according to clinical practice.

Many control algorithms have been proposed, from classic strategies to more advanced control methodologies. Different PID controllers [53, 74], predictive control [29], $H_\infty$ [60, 70, 64], sliding mode control with glucose prediction after meals [21], neural networks and fuzzy logic [76, 9], adaptative control structures [35] and algorithms inspired in the molecular biology of beta cells [59], are some of the controllers that have been tested *in silico*.

However, due to their good relation between simplicity and performance,

PID and MPC control strategies are the most used ones, and the ones which have demonstrated more clinical evidence.

## 2.3 Models in diabetes: Cobelli model

In order to obtain information related to the limitations of the closed loop systems and help patients and physicians in the understanding of the body responses to different stimulus and therapies, computer simulations using models that reflect the physiology of diabetic patients are very useful. Moreover, the *in vivo* validation of controllers without a previous *in silico* validation can lead to unnecessary risks for the patient.

So as to model the physiology of a diabetic patient body, the main parts of the organisms that take part, in one o another way, in the glucose regulation and may be affected by the disease must be taken into account. Many factors, difficult to be modelled, such as stress, exercise, the presence of infections... are present in this regulation. However, the main systems that basically govern the behaviour of a diabetic patient are:

- Insulin absorption model
- Glucose absorption model
- Glucorregulatory model

Figure 2.3 shows the block diagram of these three systems, where the outputs of the two formers act as the inputs of the glucorregulatory system.

In this diagram, the inputs are the doses (measured in insulin units ($IU$)) of insulin and the cho of the meal (measured in $gr$), entering each one in the insulin absorption model and glucose absorption model respectively. The fluxes $I_p$ (plasma insulin) and $G_{ex}$ (exogenous glucose) entering in the

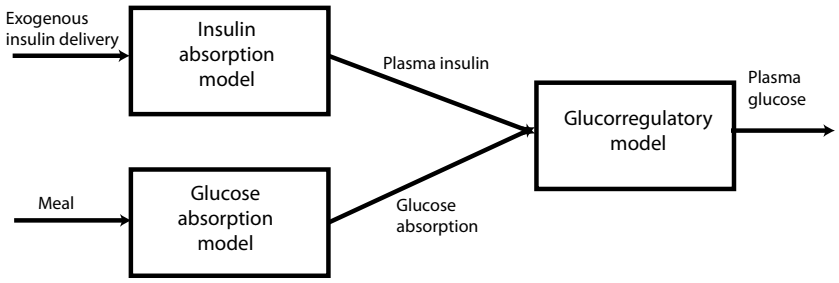


Figure 2.3: Diabetic body physiology

glucorregulatory system represent the insulin units per litre and the glucose grams per minute that enter in the organism. Finally, the output of the regulatory model is the plasma glucose concentration that can be measured by a blood sample or using a glucose sensor.

During the last years many mathematical models have been developed with different purposes, as educational models [43], models for estimating insulin sensitivity [10], and models for developing new drugs [92]. But, lately, a lot of effort is concentrating in the the development of models to test new algorithms and strategies, in virtual patients (simulation). Most of them are phenomenological models, based on prior knowledge of the physiological principles that regulate our body. In fact, in 2008 the US FDA accepted the UVa simulator developed by Virginia University as a substitute to animal trials in the preclinical testing of closed-loop control strategies.The simulator provides a set of virtual subjects based on real individual data, a simulated sensor that replicates the typical errors of continuous glucose monitoring, and a simulated insulin pump. The insulin, gastrointestinal and glucorregulatory models used in the UVa simulator are fully described in [48], [50] and [49].

Here, these models will be explained briefly since the UVa simulator will be used to validate the proposals developed in this work and its equations will be necessary to prove de SM existence in section 2.5.

**Insulin model**

The model proposed by Cobelli's group has two compartments for the interstitial space, and it considers that the elimination of insulin takes place entirely after the absorption to plasma. The structure of the model and the equations that govern it are shown in figure 2.4 and equations 2.1 respectively. Note that the elimination of insulin takes places both by degradation in the plasma compartment and in the liver, that is considered as another compartment ($I_p$ and $I_l$ respectively).

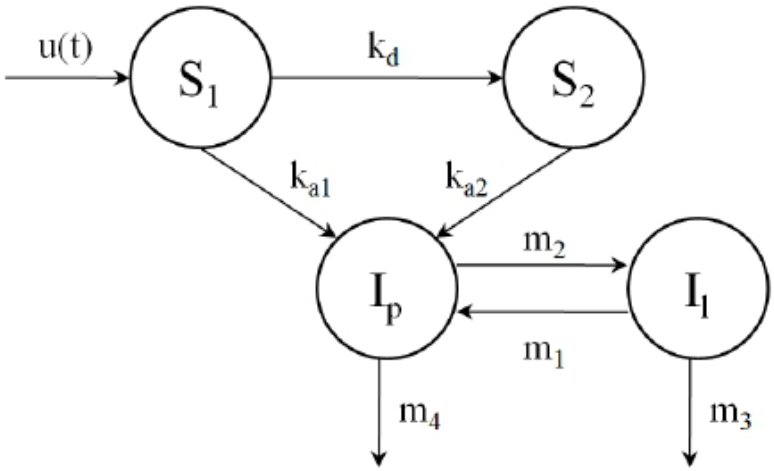


Figure 2.4: Cobelli's insulin model

$$\begin{aligned}
\dot{S}_1(t) &= -(k_{a1} + k_d)S_1(t) + u(t) \\
\dot{S}_2(t) &= k_d S_1(t) - k_{a2} S_2(t) \\
\dot{I}_l(t) &= -(m_1 + m_3)I_l(t) + m_2 I_p(t) \\
\dot{I}_p(t) &= -(m_2 + m_4)I_p(t) + m_1 I_l(t) + k_{a1} S_1(t) + k_{a2} S_2(t)
\end{aligned} \tag{2.1}$$

### Gastrointestinal

The glucose absorption model, developed by Chiara Dalla Man follows the structure shown in 2.5. This model considers a two-compartment model

for digestion and a simple single-compartmental model for the absorption in the gut.

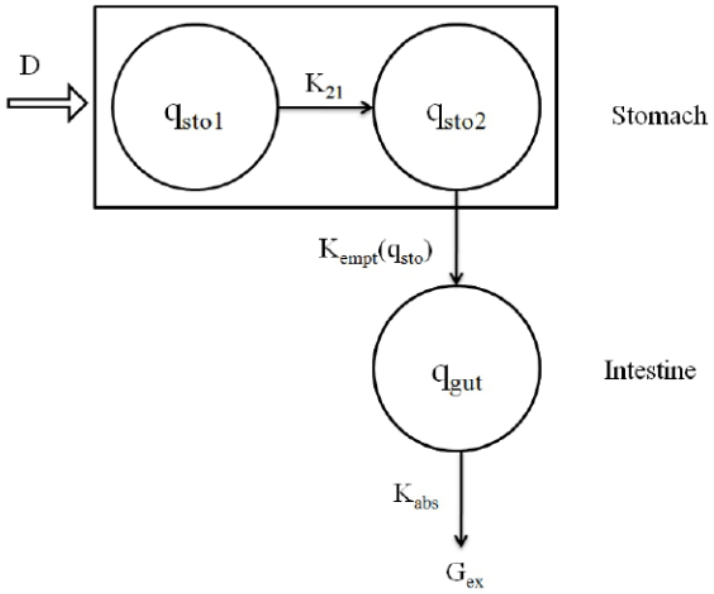


Figure 2.5: Dallaman's gastrointestinal model

The compartmental model equations are:

$$\begin{aligned}
\dot{q}_{sto1}(t) &= -K_{21}q_{sto1}(t) + D\delta(t) \\
\dot{q}_{sto2}(t) &= -K_{empt}(q_{sto})q_{sto2}(t) + K_{21}qsto1(t) \\
\dot{q}_{gut}(t) &= -K_{abs}q_{gut}(t) + K_{empt}(q_{sto})q_{sto2}(t) \\
G_{ex}(t) &= fK_{abs}G_{gut}(t)
\end{aligned} \tag{2.2}$$

where $\delta(t)$ is the Dirac delta, simulating an impulse input to the model. The rest of parameters added are flux constants, for the transfer of glucose through the system, except for the $K_{empt}$ parameter, which is time-varying and defines the form of the gastric emptying. The equations describing the transfer rate defining the flow of glucose from the stomach to the intestine are:

$$
\begin{aligned}
&K_{empt}(q_{sto}) = Kmin + \tfrac{K_{max}-K_{min}}{2} \cdot \{\tanh[\alpha(q_{sto} - b \cdot D)] - \\
&- \tanh[\beta(q_{sto} - c \cdot D)] + 2\} \\
&q_{sto}(t) = q_{sto1}(t) + q_{sto2}(t) \\
&\alpha = \tfrac{5}{2D(1-b)} \; ; \; \beta = \tfrac{5}{2Dc}
\end{aligned}
\tag{2.3}
$$

**Endogenous model**

The endogenous model is the part of the glucose-insulin model that describes the different regulatory pathways of blood glucose concentration.

The core structure of Cobelli glucorregulatory model is pretty simple, as shown in figure 2.6:

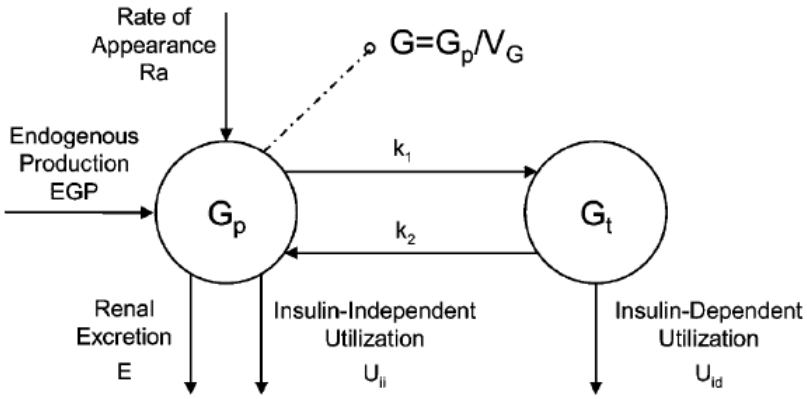


Figure 2.6: Cobelli's glucorregulatory model

The model equations are:

$$
\begin{aligned}
&\dot{G}_p(t) = EGP(t) + Ra(t) - U_{ii}(t) - E(t) - k_1 G_p(t) + k_2 G_t(t) \\
&\dot{G}_t(t) = -U_{id}(t) + k_1 G_p(t) - k_2 G_t(t) \\
&G(t) = G_p(t)/VG
\end{aligned}
\tag{2.4}
$$

Where,

- Ra is the exogenous fux of glucose coming from the gut.
- $U_{ii}$ is the utilization of glucose that is non dependent on insulin. It is usually considered constant and equal to $F_{cns}$.
- $U_{id}$ is the utilization that depends on the insulin concentration, and it follows the following set of equations:

$$\begin{aligned} \dot{X}(t) &= -p_{2U}X(t) + p_{2U}[I(t) - I_b] \\ V_m(t) &= V_{m0} + V_{mx}X(t) \\ U_{id}(t) &= \frac{Vm(t)Gt(t)}{Km+G_t(t)} \end{aligned} \tag{2.5}$$

  where X(t) is the remote insulin, I(t) is the plasma insulin, $I_b$ is the basal insulin and Vm(t) is the transfer rate for the Michaelis-Menten equation shown in equation 2.89.

- E(t) represents the renal excretion, which occurs if plasma glucose exceeds a certain threshold. Is modeled as follows:

$$E(t)=\left\{ \begin{array}{l} k_{e1}\,[G_p(t)-k_{e2}] \\ 0 \end{array} \right\} \begin{array}{l} if\ G_p(t)>k_{e2} \\ otherwise \end{array} \tag{2.6}$$

  where $k_e1$ is the glomerular filtration rate and $k_{e2}$ is the renal threshold of glucose.

- EGP(t) is the Endogenous Glucose Production, and it depends on a delayed insulin signal as follows:

$$\begin{aligned} \dot{I}_1(t) &= -k_i\,[I_1(t)-I(t)] \\ \dot{I}_d(t) &= -k_i\,[I_d(t)-I_1(t)] \\ EGP(t) &= \max\{0, k_{p1}-k_{p2}G_p(t)-k_{p3}I_d(t)\} \end{aligned} \tag{2.7}$$

  where I(t) is the insulin concentration in plasma.

A more detailed description of Dallaman-Cobelli model and other insulin-gastrointestinal-glucose models can be found in [41].

## 2.4 Set-Inversion-Based prandial insulin delivery

In this section, interval techniques explained in section 1.2 will be used to obtain prandial insulin infusion that leads to a glucose response fulfilling certain constraints.

Coming back to SIVIA algorithm (1.2.1), with a proper instantiation of the input and output spaces, $\mathbb{X}$ and $\mathbb{Y}$, and the test interval function $[t]$, it can be used to gain insight on the different dosage strategies that can be applied depending on the patient and the nature of the meal and to select the best basal-bolus combination that will yield a good postprandial control.

For this purpose, the following set inversion problem is posed:

The input space $\mathbb{X}$ corresponds to the bolus insulin dose, the modified basal insulin infusion at meal time and the time of restoration of basal to its baseline value.

For a given box in the input space, $[\mathbf{x}]$, and a set of constraints $\mathcal{C}$ on postprandial glycemia, the test function $[t]([\mathbf{x}])$ will determine whether: (1) all the insulin therapies contained in $[\mathbf{x}]$ fulfill the constraints $\mathcal{C}$ (True case); (2) none of the insulin therapies contained in $[\mathbf{x}]$ fulfill the constraints $\mathcal{C}$ (False case); (3) some of the therapies in $[\mathbf{x}]$ fulfil the constraints, while others do not (Indeterminate case).

The constraints $\mathcal{C}$ are defined here following the International Diabetes Federation (IDF) guidelines for postmeal control [36]: non-hypoglycaemia and two-hour postprandial glucose value below 140 mg/dL, in a five-hour

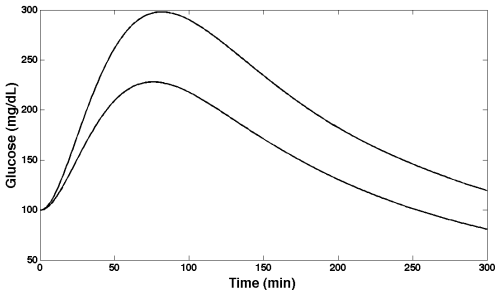


Figure 2.7: Output of an interval simulation. Upper and lower envelopes include all possible glucose responses for the input box.

time horizon. The hypoglycaemic threshold is not explicitly defined in the guidelines. A value of 70 mg/dL is adopted here. Additionally, two extra constraints are defined: five-hour postprandial glucose value above 90 mg/dL and a maximum glucose slope of 0.05 mg/dL/min starting four hours after the meal. These additional constraints are included to minimize both the risk of hypoglycaemia after the first five hours and late undesirable glucose rebounds.

Finally, a patient's model is used to predict postprandial glycemia, $G$, that is compared against the above constraints. An interval simulation of the model is carried out using Modal Interval Analysis [20]. This allows to obtain tight bounds of the envelopes enclosing the collection of postprandial glucose profiles originated from the set of therapies in $[\mathbf{x}]$. For a given time $t$, $[G](t)$ will thus be an interval (see figure 2.7). A time step of 1 minute is used in the simulation.

Remark that the above additional constraints are imposed on the model predictions, which may be inaccurate after a few hours compared to the real patient behaviour. Values were tuned accounting for this mismatch in the case of the model used here.

The test interval function, $[t]([\mathbf{x}])$ is thus defined as:

$$
\begin{aligned}
\textit{True:}\quad & (\forall t_k \in [0,300]\ [G](t_k) \geq 70) \wedge \\
& (\forall t_k \in [120,300]\ [G](t_k) \leq 140) \wedge \\
& [G](300) \geq 90) \wedge \\
& (\forall t_k \in [240,300]\ \tfrac{[G](t_{k+1})-[G](t_k)}{t_{k+1}-t_k} \leq 0.05) \\
\textit{False:}\quad & (\exists t_k \in [0,300]\ [G](t_k) < 70) \vee \\
& (\exists t_k \in [120,300]\ [G](t_k) > 140) \vee \\
& ([G](300) < 90) \vee \\
& (\exists t_k \in [240,300]\ \tfrac{[G](t_{k+1})-[G](t_k)}{t_{k+1}-t_k} > 0.05) \\
\textit{Indet.:}\quad & \text{otherwise}
\end{aligned}
$$

where $t_k$ is a discrete time instant. Remark that the above inequalities correspond to interval inequalities ($[\underline{x},\overline{x}] \leq \alpha \Leftrightarrow \overline{x} \leq \alpha, [\underline{x},\overline{x}] \geq \alpha \Leftrightarrow \underline{x} \geq \alpha,\ \alpha \in \mathbb{R}$).

The kind of inner subpavings that are obtained after the application of the algorithm is shown in figure 2.8 (left). The subpaving consists of 3D feasible boxes, where these three dimensions correspond to the bolus dose, the postprandial basal dose and time of restoration of basal to baseline. The 2D basal-bolus projection (figure 2.8 right) contains information on the different basal-bolus combinations that will lead to a good performance for a particular patient and meal. In this way, combinations in the inner subpaving are guaranteed (with a proper selection of the time of restoration of basal to baseline) to yield a glucose profile that fulfills the defined constraints. On the contrary, combinations outside the outer subpaving will violate some constraint (see figure 2.9). If the outer subpaving is empty, there is no solution to the problem unless the constraints are relaxed.

The projected basal-bolus space can be divided into regions corresponding to different bolus administration modes present in current insulin pumps, plus a new one called here temporal basal decrement (see figure 2.10). This

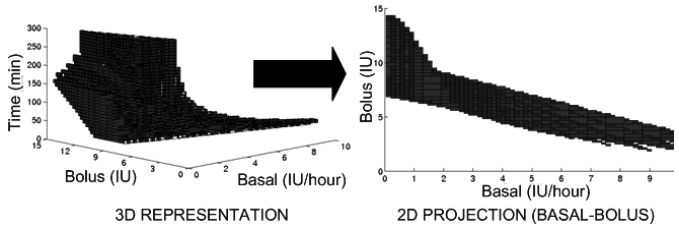


Figure 2.8: Plot that represents a 3D (basal, bolus and time) feasible set with its corresponding basal-bolus 2D projection.

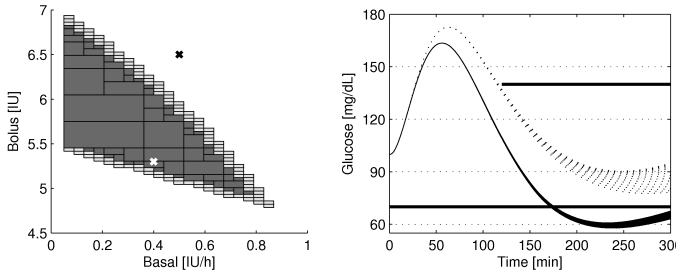


Figure 2.9: Plot that shows the glucose response for a basal-bolus combination inside the inner subpaving (dotted line) and for a combination outside the outer subpaving (solid line). The glucose response has been represented for times of restoration from 30 to 300 min demonstrating that for combinations in the inner subpaving always exists at least one solution, selecting the appropriate time of restoration of basal from the feasible set, that fulfills the constraints whereas, for combinations outside the outer subpaving is impossible to obtain a proper glucose control.

is especially important since it allows the automatic selection of the best administration mode. So far this is done based on the physician's heuristics. To ease interpretability, a normalization is done with respect to the patient's nominal basal and standard bolus from its insulin-to-carbohydrate ratio (I:C). The point (1,1) corresponds thus to the standard therapy.

Figure 2.10 shows a situation where all the different bolus administration modes (standard bolus, square bolus, dual-wave bolus and temporal basal decrement) will result in a good glucose response, fulfilling the IDF guidelines of postmeal control. Depending on the patient and on the grams of carbohydrates of the meal, the number of bolus modes fulfilling the constraints may be reduced.

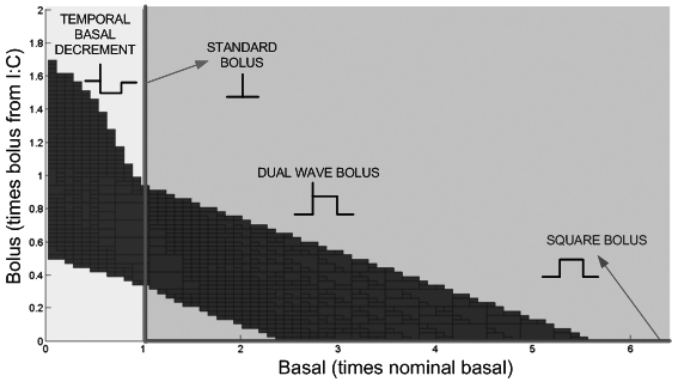


Figure 2.10: Normalized feasible set that shows all the possible bolus administration modes. Therapies with nominal basal correspond to a standard strategy, therapies with an increment in basal postprandial dosage result in a dual-wave or square-wave strategy whereas therapies with less postprandial basal than baseline are called here as temporal basal decrement mode. The corresponding insulin infusion profiles are depicted for each region.

The procedure used to select a specific point (basal-bolus combination) from all the possible ones is done as follows. The 2D basal-bolus subpaving is divided into two smaller subpavings (when possible) corresponding to a positive and negative basal deviation from nominal. The first one will correspond to a bolus mode currently available in insulin pumps (standard/square/dual-wave). The second one will correspond to a new administration mode, found to be the only solution for big sized meals (see [6]). The optimal point of each of these new subpavings can be selected in several ways, and different approaches will be explained here:

- Centroid solution: The basal-bolus combination is chosen as the geometric centroid of the corresponding subset. This alternative leads to a conservative solution where the glucose response remains as far as possible from the constraints. Although this solution does not optimize the glucose profile, it is the most robust solution against mismatches between patients? model and actual patients.

- Maximal-bolus solution: The basal-bolus combination is chosen by

applying the highest possible bolus to optimize the 2-hour postprandial glucose concentration. This solution follows a similar philosophy to the typical physicians' approach for selecting the appropriate I:C ratio for each patient. The difference here is that the coordinated basal-bolus action will allow an optimal 2-hour postprandial glucose control, while avoiding hypoglycaemia.

After the selection of the desired basal-bolus combination, the time of restoration of basal to baseline is selected from the third dimension in the 3D feasible set, which corresponds to an interval of feasible times of restoration. The mid-value is considered here.

**Patient's model identification**

The algorithm requires obtaining an individual model for each of the patients, characterizing their postprandial glucose behavior. PAtients used here are the virtual patients in UVa simulator. UVa simulator uses the Cobelli model as a mathematical description of type 1 diabetic patients. In order to force mismatch between patient's model and the virtual patient behavior, the Hovorka model [32, 31] structurally different, is used as patient's model. Its parameters are identified from 4-day virtual patient's data for a period of five hours after a meal, following an optimal experiment design (OED) [45, 87]. The set-up parameters considered in the OED are the ingested amount of carbohydrates, the bolus insulin dose and the time instant of bolus insulin infusion. Constraints are added to avoid glucose concentrations below 70 mg/dL or above 300 mg/dL. The experiment can be carried out in ambulatory conditions. The optimality criterion used in this study is D-optimality, corresponding to the maximization of the determinant of the Fisher information matrix [87].

The use of a model structurally different than the model used in the UVa simulator is justified by the unavoidable discrepancies that always exist between the real behaviour of a patient and the response of its model.

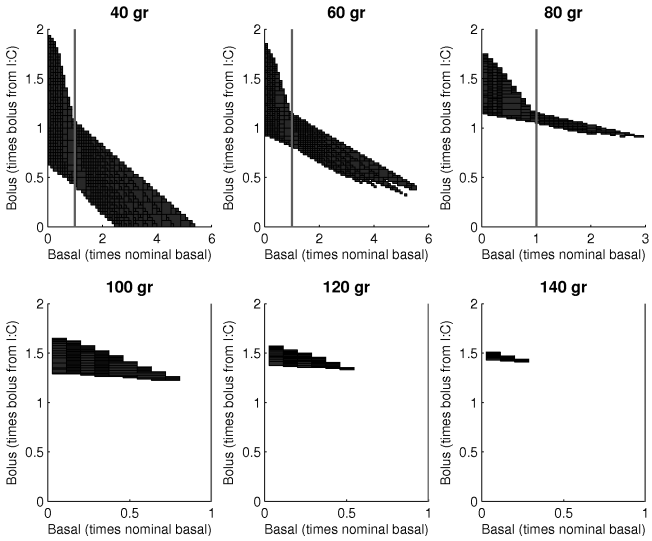


Figure 2.11: 2D basal-bolus projection of normalized feasible sets for a meal of 40 to 140 grams of carbohydrates and initial normoglycemia. The vertical line stands for the standard strategy with basal equal to its baseline value.

Choosing a different model for identification than the one used in the simulator allows evaluating the robustness of the algorithm with respect to model and patient mismatch.

### Validacion

Once the model is obtained, the normalized 2D basal-bolus projections are computed for meals in the range 40-140 grams of carbohydrates and initial normoglycemia. Figure 2.11 shows the results obtained for one representative virtual patient.

The most remarkable issue extracted from figure 2.11 is that for low carbohydrate content meals ($<$ 80 gr), different possible strategies lead to a good glucose control whereas as the carbohydrate content increases, the set of possible solutions is reduced, as expected. For big sized meals ($>$ 100 gr), only a temporal basal decrement strategy with an increment in the bolus dosage with respect to nominal ("a superbolus therapy" [85, 86]) can yield to a good postprandial control. Similar behavior can be observed in the rest of

the patients being, the temporal basal decrement strategy the only strategy that provides good results for big sized meals. Occasionally, for a particular meal and patient, the feasible set could be empty, in which case the upper constraint will be relaxed in steps of 20 mg/dL to a maximum of 300 mg/dL.

In order to check the results obtained in figure 2.11, an intermediate sized meal (60 gr) and a big sized meal (120 gr) are selected to compare the glucose response applying the basal-bolus insulin combinations given by the algorithm for each possible bolus administration mode with the response using the standard therapy (see figure 2.12). The centroid solution for the selection of an specific basal-bolus combination from all the possibles is used. For the 60 gr meal any of the three possible therapies (standard, dual-wave and temporal basal decrement) yields a good performance whereas for the 120 gr meal, the basal-bolus combination given by the algorithm using a temporal basal decrement strategy improves significantly the performance of the standard therapy, incapable of fulfilling the IDF guideless for postprandial control. In this case, both strategies could produce a very mild hypoglycemia seven hours after the meal [8]. However, this is not at all critical.

See [68] for a thorough comparison of the results obtained for the 30 available virtual patients in the UVa Simulator (adults, adolescents and children) using the centroid solution and the maximal-bolus solution.

## 2.5 Use of an additional SMRC loop to deal with IOB constraints

In this section, the second proposal advanced in the introduction is explained in detail. The main objective here is to limit the concentrations of residual

[8] There is no consensus about the hypoglycemic threshold. Some clinicians use a value of 60 mg/dL. Here, a more restrictive value of 70 mg/dL was used.

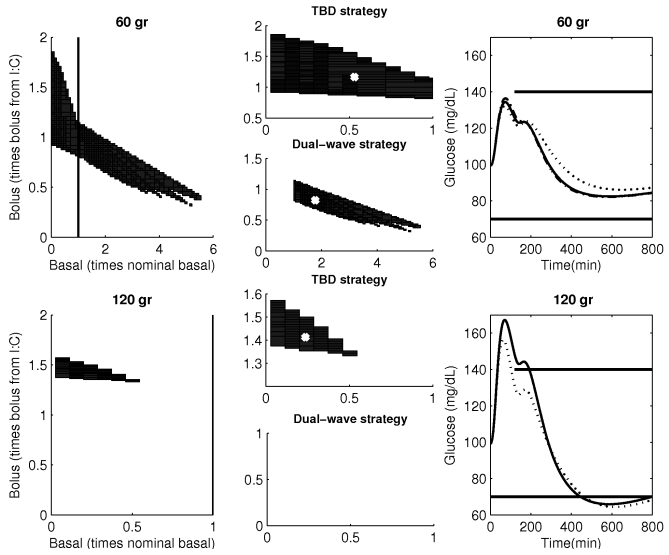


Figure 2.12: Comparison among the postprandial glucose profiles applying different therapies for 60 and 120 gr meals. The subpavings corresponding to each bolus administration mode are represented (when existing) separately. The specific basal-bolus combination selected for each strategy is showed in the subpavings as a thick dot. Finally, the glucose response using the basal-bolus combinations given by the algorithm and the standard therapy are plotted. The solid line corresponds to the standard therapy, computed from the I:C ratio given by the UVa simulator, whereas the dotted line and the dotted-dashed line represent the temporal basal decrement (TBD) and the dual-wave therapy respectively. The horizontal lines represent the IDF constraints.

insulin (IOB) with the objective of preventing hypoglycaemia. Indeed, that is a question not solved yet by the closed-loop strategies found in literature.

It is assumed we have a patient controlled using a conventional PID (for instance [74])[9]. As the insulin on board is inaccessible and difficult to measure, it must be estimated. For doing this, Cobelli's model of the insulin subsystem is used. In that way, from equation 2.1, the IOB can be represented as $S_1 + S_2$.

[9]Note that the controller could be whatever, since the additional SMRC loop is independent of the main loop

A representation of the proposed closed loop scheme is shown in figure 2.13 where the inner controller (C) can be expressed in its ideal form as 2.8.

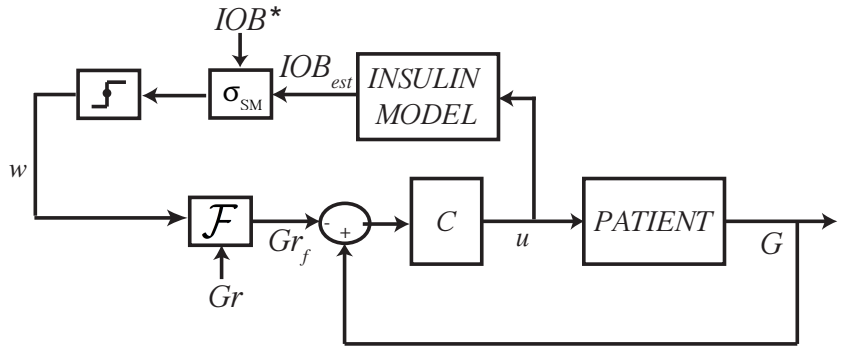


Figure 2.13: SMRC implementation for diabetes application

$$u(t)=K_P e(t)+\frac{K_P}{\tau_I}\int_0^t e(\tau)d\tau+K_P\tau_D\frac{de(t)}{dt} \tag{2.8}$$

where $e = G - Gr_f$. Notice when u(t) (insulin injected) increases, the glucose concentration G decreases. This fact explains the error sign.

In order to avoid abrupt changes in $u$ due to changes in the reference, and due to the fact that for postprandial control, the constant $\tau_I$ is very large, the realizable expression of the controller used for calculation and implementation is:

$$u(t)=K_P e(t)+K_P\tau_D\frac{\mathrm{dG(t)}}{\mathrm{dt}} \tag{2.9}$$

The additional SMRC loop consists of two main elements. A discontinuous decision block responsible for remaining IOB inside the desired bounds and a first order filter $F$ which purpose is to smooth out the conditioned reference.

The first order filter takes the form:

$$\dot{Gr}_f = -\alpha \left( Gr_f + w - Gr \right), \tag{2.10}$$

where $G_r$ is the desired reference when IOB does not reach the defined bounds, $Gr_f$ is the conditioned reference when the SMRC loop is active, $\omega$ is the discontinuous signal and $\alpha$ is a design parameter.

Combining the expressions related to IOB of the insulin system (2.1), the controller (2.9) and the filter (2.10), the complete system can be rewritten following 1.34 as:

$$\begin{pmatrix} \dot{S}_1 \\ \dot{S}_2 \\ \dot{u} \end{pmatrix} = \begin{pmatrix} (-\mathrm{k_{a1}}-\mathrm{k_d})S_1+u \\ k_d S_1+k_{a2} S_2 \\ k_P \alpha G r_f \end{pmatrix} + \begin{pmatrix} 0 \\ 0 \\ k_P \alpha \end{pmatrix} w + \begin{pmatrix} 0 \\ 0 \\ k_P \dot{G}+k_D \ddot{G}-k_P \alpha G r \end{pmatrix} \tag{2.11}$$

where $x = \begin{pmatrix} S_1 \\ S_2 \\ u \end{pmatrix}$, $f = \begin{pmatrix} (-\mathrm{k_{a1}}-\mathrm{k_d})S_1+u \\ k_d S_1+k_{a2} S_2 \\ k_P \alpha G r_f \end{pmatrix}$, $g = \begin{pmatrix} 0 \\ 0 \\ k_P \alpha \end{pmatrix}$

and $p = \begin{pmatrix} 0 \\ 0 \\ k_P \dot{G}+k_D \ddot{G}-k_P \alpha G r \end{pmatrix}$

Defining IOB as $S_1+S_2$ the relative degree from IOB to the discontinuous signal w is gr=2. Moreover, the terms that are seen as perturbation are collinear with the discontinuous signal $w$. Notice these terms represent the dynamics of the glucose. That is, the inner loop is seen as a perturbation.

Two constrains for the IOB are defined. One upper constraint to solve, as explained before, the problem of hypoglycaemia incidence, and an additional

lower constraint to avoid undesirable glucose rebounds and maintain a minimum quantity of IOB. Hence, the sliding surfaces will be defined as follows:

$$\sigma_1=(S_1+S_2)-\overline{IOB}+\tau\frac{d(S_1+S_2)}{dt} \tag{2.12}$$

$$\sigma_2=(S_1+S_2)-\underline{IOB}+\tau\frac{d(S_1+S_2)}{dt} \tag{2.13}$$

being the switching logic:

$$w=\left\{\begin{array}{c} w^+ \; if \; \sigma_1>0 \\ w^- \; if \; \sigma_2<0 \\ 0 \; otherwise \end{array}\right\} \tag{2.14}$$

Note that, because of the way the system is defined, $w^+$ will be negative and $w^-$ positive. That is, when the upper bound is going to be violated, the reference value is incremented so as to diminish the control action, and vice versa for the lower constraint. In other words, when $\sigma_1 > 0$, IOB is higher than $\overline{IOB}$. In order to decrease IOB, the insulin injected (u) must decrease (see equation 2.11). This effect is achieved increasing $Gr_f$ leading to higher levels of blood glucose and avoiding hypoglycaemia due to an excess of insulin. In the same way, when when $\sigma_2 < 0$, IOB is lower than $\underline{IOB}$ and $Gr_f$ must decrease in order to force an increment in u and inject more insulin. This procedure will avoid undesirable later glucose rebounds once the effect of the meal has already been counteracted.

From 1.3.2, the existence condition that must be fulfilled so as the sliding mode to exist, is the trasversality condition, that is $L_g\sigma = \frac{\partial\sigma}{\partial x}g \neq 0$. As, $L_g\sigma_1 = L_g\sigma_2$, calculations will be developed for $\sigma_1$, being the procedure for $\sigma_2$ analogous.

$$\frac{\partial \sigma_1}{\partial \mathrm{x}} = \begin{pmatrix} 1-\tau(k_{a1}+k_d) & 1+\tau k_{a2} & \tau \end{pmatrix} \tag{2.15}$$

$$L_g\sigma_1 = \frac{\partial \sigma_1}{\partial x} g = \begin{pmatrix} 1-\tau(k_{a1}+k_d) & 1+\tau k_{a2} & \tau \end{pmatrix} \begin{pmatrix} 0 \\ 0 \\ k_P\alpha \end{pmatrix} = \tau k_P \alpha \tag{2.16}$$

where $k_P$, $\tau$ and $\alpha$ are design parameters, always different from 0 and positive. Therefore, the transversality condition holds.

In order to follow the invariance condition stated in 1.3.2, and according to 1.39,

$$(w^+ - w^{\sigma_1}) L_g\sigma_1 \leq 0, \forall \mathbf{x} \in \partial\Phi \Longrightarrow \tag{2.17}$$

Since in this case $L_g\sigma_1 > 0$, $w^+$ must be chosen to fit equation:

$$w \leq w^{+\sigma_1} = -\frac{L_f\sigma_1}{L_g\sigma_1} \tag{2.18}$$

with,

$$w^{\sigma_1} = \frac{\mathrm{S_1}(\mathrm{k_{a1}} - \tau(\mathrm{k_{a1}}^2 + 2\mathrm{k_{a1}k_d} + \mathrm{k_d}^2 + \mathrm{k_{a2}k_d})) + \mathrm{S_2}(-\mathrm{k_{a2}} - \tau\mathrm{k_{a2}}^2) + \mathrm{u}(\tau\mathrm{k_{a1}} + \tau\mathrm{k_d} - 1) - \tau\mathrm{k_P}\alpha\mathrm{Gr_f}}{\tau\mathrm{k_P}\alpha} \tag{2.19}$$

Recall $w^+$ will be negative. So, in order to fit equation 2.18, $w^{\sigma_1}$ must be negative and lower bounded. The states of the systems $S_1$, $S_2$ are always

positive and also $u$ (we cannot "extract" insulin and the inner loop is designed according to this constraint). Therefore,

$$w^{\sigma_1}=\xi_1 S_1-\xi_2 S_2-\xi_3 Gr_f+\xi_4 u \tag{2.20}$$

with $\xi_2 > 0$ and $\xi_3 > 0$. In tha way, defining properly $\tau$, $\alpha$ and $w$ equation 2.18 can be fulfilled.

**Dealing with inter-patient variability**

As it was said in sections 2.2 and 2.3 a lot of variability from one patient to other exists. In order to deal with variability, different upper limits for IOB are defined depending on an estimation of the insulin sensitivity of each patient. This estimation is carried out by computing the total daily dose of insulin (IDD) (from his basal insulin rate).

The structure that will be follow for the main control loop is the one showed in 2.2, with meal announcement. In this case, a fixed 2IU bolus will be infused in the instant of the meal. So, the meal announcement will only indicate the time of the meal, but neither the quantity nor the composition of it. Obviously, the upper limit for IOB needs to be different depending on the grams of cho and also on the absorption of the meal. To deal with these issues, another criterion to determine $\overline{IOB}$, is established. It will be higher for meals that cause a large glucose slope (supposed to be a big meal) and lower for lower glucose slopes. The glucose slope will be determined using glucose measures at the meal time and ten minutes later.

By using those two criteria (IDD and glucose slope) six different upper limits for IOB will be defined ranging from 5 to 15 IU. Additionally, these limits are reduced, if they are caused by the second peak of the meal absorption or if the patients initial condition is moderate hypoglycaemia (values bellow 80 mg/dL). Additionally, initial conditions of hyperglycaemia will allow higher concentrations of IOB.

In order to maintain always a minimum of IOB to keep a good basal glucose concentration, a fixed lower bound for IOB is established for all the situations.

Remark that although $\overline{IOB}$=$\overline{IOB}(G, \dot{G}, t)$, $\overline{IOB}$, it is not strictly time variable. Its value is defined at the beginning of a meal and remains constant until a second glucose peak is detected or another meal takes place. It is a constant interval function with $\dot{\sigma}_1$=$\dot{\sigma}_2$=0.

**Simulations and Validation**

An example of the kind of results obtained with this algorithm is shown in figures 2.14 and 2.15. In these figures the glucose profile obtained with a PID tuned for avoiding hypoglycaemia (conservative PID), with a more aggressive PID where the main objective is to reduce the time stayed in hyperglycaemia, and with this same controller with constraints in IOB is shown. In figure 2.14 it can be seen how the addition of the SMRC loop allows the implementation of an aggressive control but preventing hypoglycaemia. In that way, this loop can be seen as a security system. Figure 2.15 shows the periods when the SMRC is active and how it is capable of keeping the insulin on board bellow the defined upper bound.

Figure 2.16, where the $S_1$ and $S_2$ trajectories on phase are plotted, illustrates how the SMRC acts. It forces the limited variable (in this case IOB)not to exit the specified surface, leaving it free when it remains inside it.

So as to evaluate how robust the strategy is, the acceptable difference that can exist between the estimated IOB and the real one to obtain a glucose profile within prescribed bounds is evaluated. To do this, an optimization problem was set up. The optimization was carried out in a virtual patient with medium parameters, and the objective was to see how different could be the real IOB parameters ($k_{a1}$, $k_{a2}$ and $k_d$) from the ones used for IOB

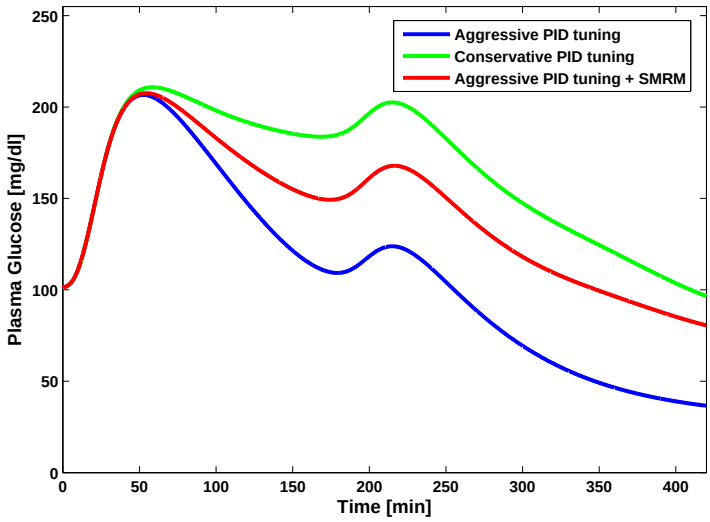


Figure 2.14: Glucose profile using three different strategies

| | $k_{a1}$ | $k_{a2}$ | $k_d$ |
|---|---|---|---|
| CV (%) | 78 | 77 | 81 |

Table 2.1: Allowed CV for each parameter

estimation to still avoid hypoglycaemia and obtain basal glucose after 5 hours near 100 mg/dL.

The optimization reveals that a difference near 80% between the medium parameters used for estimation and the real ones still provides good glucose responses. Table 2.1 shows the specific result for each parameters.

The evaluation of the above explained methodology has been carried out through an *in silico* study using the 10 adult virtual patients available in the educational version of the Food and Drug Administration-accepted University of Virginia simulator.

Table 2.5 shows the demographic, anthropometric, and metabolic parameters of the 30 patients. Nominal basal is taken as the basal infusion

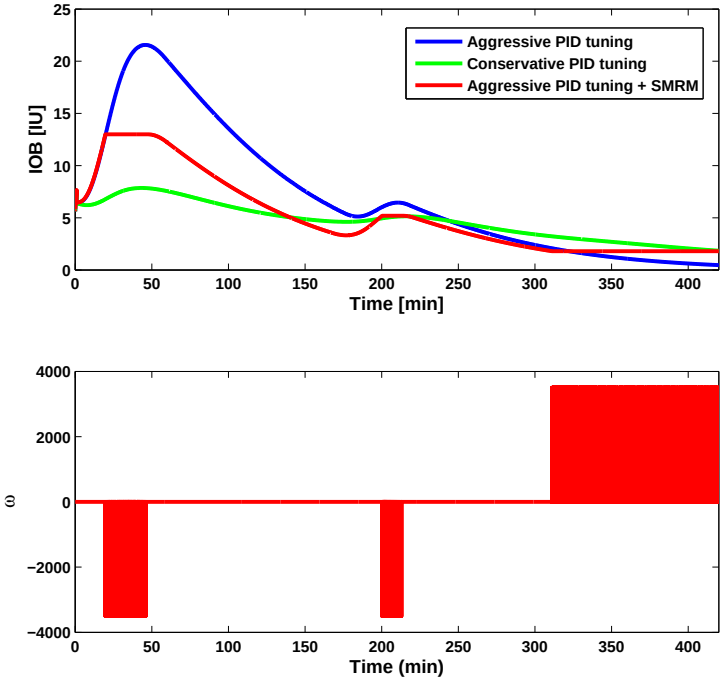


Figure 2.15: IOB and discontinuous signal

| | Age | Weight (kg) | Nominal basal (IU/hour) | I:C (g/IU) |
|---|---|---|---|---|
| Mean | 51.6 | 86.07 | 1.685 | 9.92 |
| Standard deviation | 16 | 15.79 | 0.25 | 6.33 |

Table 2.2: Demographic, Anthropometric, and Metabolic Parameters of the 10 in Silico adult Subjects Available in the Educational Version of the University of Virginia Simulator

normalizing glucose around 100 $mg/dl$, and the insulin-to-carbohydrate ratio (I:C) is estimated through simulations trying to obtain a 2 h glucose concentration below 140 $mg/dl$.

By using these cohort of patients, the performance of the algorithm in the presence of inter-patient variability is evaluated. To incorporate to this validation the effect of intra-patient variability, sinusoidal oscillations of 5%

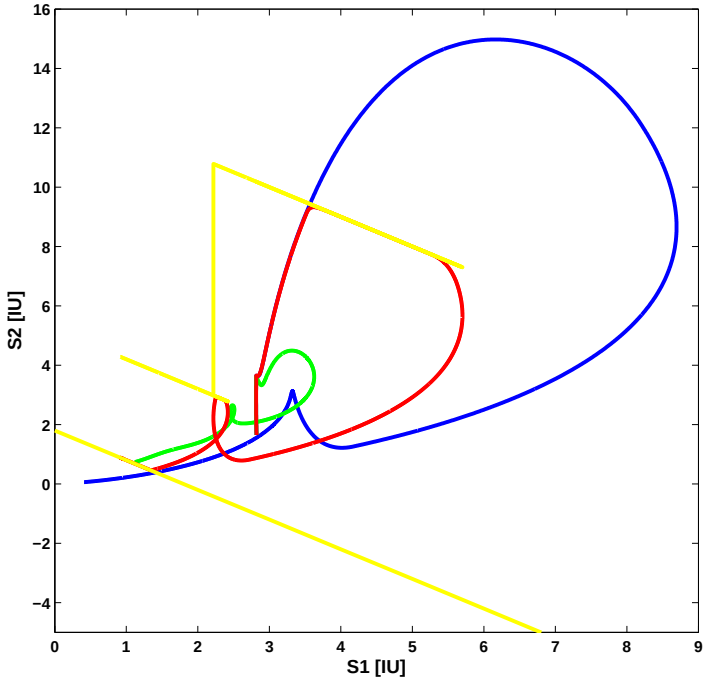


Figure 2.16: S1 and S2 trajectories on phase plane with the aggressive PID (blue), the conservative PID (green) and the aggressive PID with the SMRC loop (red). The yellow lines represent the variable IOB upper bound and the fixed IOB lower bound. Remember $IOB = S_1 + S_2$

amplitude and 3 h period has been a superimposed in nominal values of selected model parameters similar than in [89]. Each of those parameters had a different phase generated randomly from a uniform distribution U[0,3 h].

Ten simulations for each patient were carried out following a 16h clinical protocol corresponding to active daily hours (from 8h to 24h) and three meals (8:00 am, noon, and 6:00 pm) with 20, 80, and 120 g of cho. For each of these simulations three control strategies, conservative PID, aggressive PID and aggressive PID plus an addition SMRC loop that impose constraints on the IOB have been evaluated and compared. In table 2.5 the mean

| | % of time G>180 mg/dL | | | % of time G<60 mg/dL | | |
|---|---|---|---|---|---|---|
| | $PID_{con}$ | $PID_{aggr}$ | $PID_{aggr} + SMRC$ | $PID_{con}$ | $PID_{aggr}$ | $PID_{aggr} + SMRC$ |
| pac 1 | 34.85 | 2.57 | 7.85 | 0 | 7.48 | 0.47 |
| pac 2 | 29.1 | 2.91 | 5.52 | 0 | 0.27 | 0 |
| pac 3 | 21.29 | 0.93 | 12.21 | 0 | 19 | 2.46 |
| pac 4 | 19.07 | 6.93 | 7.67 | 0 | 55.21 | 45.54 |
| pac 5 | 28 | 8.21 | 14.08 | 0 | 4.2 | 1.22 |
| pac 6 | 32.65 | 5.39 | 18.62 | 9.55 | 38.21 | 18.86 |
| pac 7 | 20.38 | 0 | 3.49 | 0 | 18.51 | 1.64 |
| pac 8 | 16.34 | 0.19 | 1.15 | 0 | 17.99 | 0 |
| pac 9 | 60.69 | 13.43 | 45.55 | 0 | 0 | 0 |
| pac 10 | 38.9 | 16.45 | 30.10 | 0 | 9.29 | 0.70 |

Table 2.3: Percentage of time in Hypo and Hyperglycaemia with the 3 control strategies

percentage of time above 180 mg/dL and the percentage of time below 60 mg/dL for each patient and each strategy is shown. Remark that although with the conservative PID hypoglycaemia is avoided (it was designed for that purpose), in all of the 100 simulation performed, the glucose profile reached values above 180 mg/dL, remaining there 30% of the time whereas with the aggressive PID only 6% of the total simulation time was above those glucose values. The aggressive PID with the additional SMRC, continues offering a good hyperglycaemia performance (14% of the total simulation time) but reduces the hypoglycaemia events considerably (7% of the total time of the simulations versus 17%) and also the events registered are events of moderated hypoglycaemia.

Figure 2.17 shows the mean glucose profile of the 100 simulations performed. It can be see that the aggressive PID plus SMRC represents a compromise solution between a strategy of avoiding hypoglycaemia with the risk of keeping glucose values too high for a long time, and the more aggressive strategy where the hypoglycaemia risk is unaffordable.

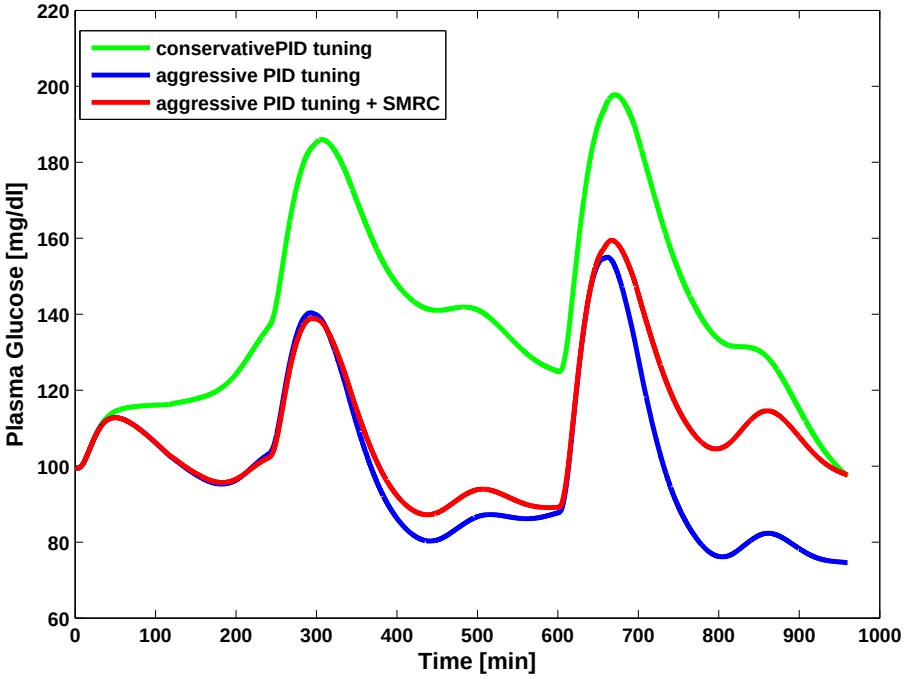


Figure 2.17: Mean glucose profile of the 10 adult patients using the three strategies presented

## 2.6 Discussion and future work

In this chapter two proposals related in certain way to glucose control of processes subject to constraints are presented.

In the first one, an algorithm for calculating the most appropriate combination of basal and bolus insulin for a good postmeal glucose control is thoroughly presented. The set inversion methods based on interval analysis are applied to determine, for a given meal, which bolus-administration mode will yield a glucose response fulfilling the IDF guidelines of postprandial control. Clinical trials to evaluate the efficacy of the algorithm *in vivo* are currently ongoing.

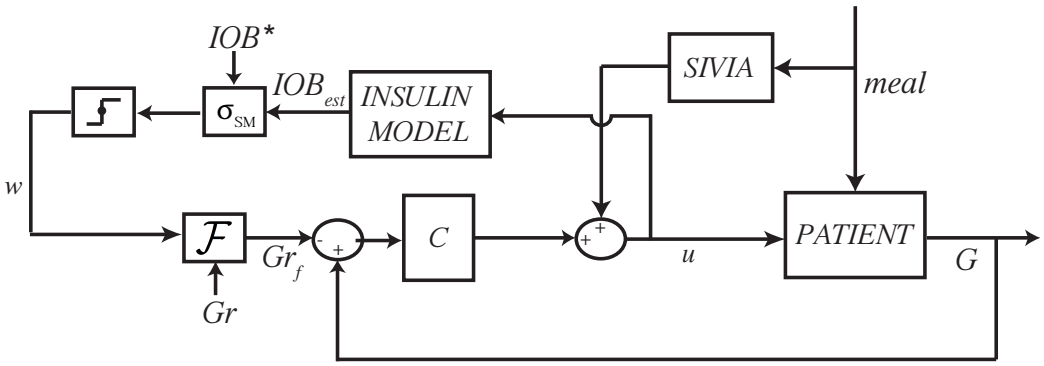


Figure 2.18: Glucose closed loop system implementation wuth SIVIA as feed-forward algorithm and an additional SRMC loop

A strength of the proposed method is its robustness. The use of a model significantly different than the virtual patient for the identification of the patient's postprandial behavior shows the feasibility of the method in spite of imperfect glucose predictions, due for instance to intra-patient variability. Robustness of the solution could be further increased, if needed, with explicit consideration of intra-patient variability (as interval quantities in model parameters) in the computation of the feasible solution set with SIVIA (that would yield smaller feasible sets and thus more constrained solutions). This is a unique feature of the presented algorithm. Another one is the possibility of determining, in a non-heuristic way, the feasible insulin administration modes for a given meal, which could be included in smarter insulin pumps in the future.

The second proposal consisted in adding to a closed loop glucose system, restrictions in the IOB present in the patients body during the control, using concepts of SMRC. Potentiality of the use of constraints in the IOB has been already demonstrated in [19]. The main advantage of this new approach presented here, is that the additional security SMRC loop that limits the IOB is independent of the inner control loop. In that way, it can be added to any existing closed control loop giving more confidence about its good hypoglycaemia performance.

The upper and lower IOB bounds can be defined by the physician based on his knowledge and it can be also adjusted in an adaptive way, in the same way that it is done usually with the open loop insulin therapy to adapt them to the behaviour of an specific patient.

Another interesting application of this strategy could be its use for tuning controllers automatically. The percentage of time that the SMRC loop is activated, could be translated into changes in the controller parameters so as to relax it and do it less aggressive if those percentages are too high.

Finally, as future work, both proposals presented in this chapter could be combined. Note that in the SMRC proposal, a fixed feed-forward control action (2 IU) is given each meal. Better results could be obtained with a more sophisticated feed-forward control. As future work, the study of the integration of SIVIA algorithm in the closed loop system with an additional SMRC loop, acting SIVIA as feed-forward control must be carried out. Figure 2.18 shows the proposed closed loop system implementation combining these both strategies.

Chapter 3

# Limiting ethanol flux in *Saccharomyces cerevisiae*

## 3.1 Introduction

According to the Office of Technology Assessment [58], biotechnology can be defined as "*commercial techniques that use living organisms, or substances from those organisms, to make or modify a product, and including techniques used for the improvement of the characteristics of economically important plants and animals and for the development of microorganisms to act on the environment*". Following this definition, biotechnology has existed for a long time. For centuries, people have been using microorganisms to ferment and obtain beverage and food. Due to its potentiality, scientists have shown much interest in understanding the reactions that take place inside the microorganisms in order to exploit their capabilities. Nowadays biotechnology is applied to numerous fields such as, pharmaceuticals, agriculture, chemical applications, environmental applications and bioelectronics.

In many biotechnological processes, the optimal productivity corresponds

to operating at critical substrate concentration that can be regulated by controlling the feed rate [81, 57]. Typically, this critical substrate value changes from experiment to experiment and from strain to strain, and even in the same experiment due to changing environmental and/or process conditions. Moreover, if constraints are present (*e.g.* due the production of additional toxic or inhibitory metabolites) the optimal point may not correspond to a maximum of the kinetic rates.

This is the case, for instance, when dealing with the optimal production of biomass in *Saccharomyces cerevisiae*. *Saccharomyces cerevisiae* is a well-studied eukaryotic system commonly used for making bread, alcohol and recombinant proteins. It is one of the yeast species classified as "glucose sensitive" which means that they may produce ethanol also under aerobic conditions when the sugar concentration is high. This phenomenon is also known as overflow metabolism [66, 73]. In this case, the optimal production of biomass avoiding the production of ethanol remains below the maximum attainable specific growth rate.

In this way, the problem consists in finding the feeding rate which gives the closest specific growth rate to the desired one and which is compatible with the critical constraint, so as to avoid overflow metabolism[1].

Several methods have been proposed in the literature to deal with this problem [13, 1]. In [62] SMRC is already used to optimize the biomass specific growth rate of *Saccharomyces cerevisiae* compatible with constraints in the etahnol concentration. Here, a similar procedure where the constrained variable is not the ethanol concentration but the ethanol flux is applied. This work will allow future work in two directions. On one hand the control of internal fluxes which can not be measured and need to be estimated and, on

[1]Similar problems could be the need of achieving an optimal behaviour of a microorganism according to an objective (maximizing the protein expression, the biomass growth rate, the efficiency of the biorreaction) subject to constraints in certain fluxes. Reasons could be the presence of metabolites that are toxics or inhibitors or the need to force the metabolism to follow a preferential path.

the other hand the fact of taking into account uncertainty in the measures that lead to interval or possibilistic flux estimations [47].

In section 3.2 a description of the model of *Saccharomyces cerevisiae* that is going to be used is provided. Section 3.3 deals with technical details of the SMRC inplementation. In section 3.4 a set of simulations are presented and, finally, section 3.5 is a discussion and future work premises.

## 3.2 *Saccharomyces cerevisiae model*

The model of *Saccharomyces cerevisiae* that will be used in this work is a widely accepted model proposed by Sonnleitner and Kappeli [73]. It is called the bottleneck principle model and it assumes a limited respiratory capacity of the cells. The mass balanced macroscopic model is presented in equation 3.1.

$$\begin{aligned} \dot{x} &= (\gamma_1 r_1 + \gamma_2 r_2 + \gamma_3 r_3)x - x\frac{F}{v} \\ \dot{s} &= -(r_1 + r_2)x + (s_i - s)\frac{F}{v} \\ \dot{e} &= (\gamma_4 r_2 - r_3)x - e\frac{F}{v} \\ \dot{v} &= F \end{aligned} \tag{3.1}$$

where x, s and e are the concentrations of biomass, substrate and ethanol. v and F are the volume and the inlet flow.

Biomass is produced through three paths: oxidation of glucose, reduction of glucose, and oxidation of ethanol, represented by the kinetic terms $r_1$, $r_2$ and $r_3$, respectively. These reactions rates and the kinetics terms are shown in 3.2 and 3.3. Table 3.2 presents typical values for the parameters in those equations.

$$
\begin{aligned}
r_1 &= \min\left(r_s, \frac{r_o}{\gamma_5}\right) \\
r_2 &= \max\left(0, r_s - \frac{r_o}{\gamma_5}\right) \\
r_3 &= \max\left(0, \min\left(r_e, \frac{r_o - \gamma_5 r_s}{\gamma_6}\right)\right)
\end{aligned} \tag{3.2}
$$

$$
\begin{aligned}
r_s &= \mu_{m,s}\frac{s}{k_{s,s}+s} \\
r_e &= \mu_{m,e}\frac{e}{k_{s,e}+e} \\
r_o &= \mu_{m,o}\frac{o}{k_{s,o}+o}
\end{aligned} \tag{3.3}
$$

Figure 3.1 shows a graphical description of the overflow metabolism.

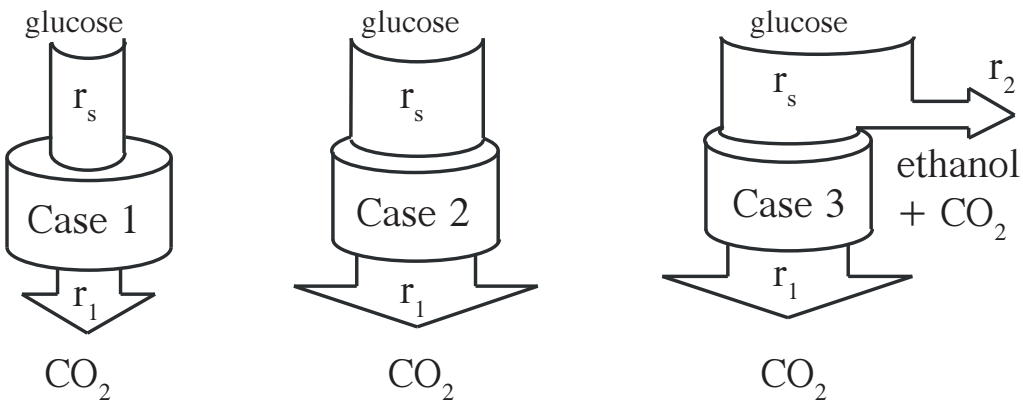


Figure 3.1: Overflow metabolism representation [73]

For Case 1, there is excess capacity and no metabolite is formed. Case 2 represents growth at the critical rate where any excess substrate would "overflow" to ethanol. In Case 3, the excess growth above the critical rate is represented by the ethanol flux.

Using standard notation and considering an exponential feeding law $F{=}\lambda xv$, with the gain $\lambda$ to be determined by the control objective, the model 3.1 can be written as:

| $\gamma_1$ | $\gamma_2$ | $\gamma_3$ | $\gamma_4$ | $\gamma_5$ | $\gamma_6$ |
|---|---|---|---|---|---|
| 0.49 | 0.005-0.12 | 0.5-1.2 | 0.48 | 0.396 | 1.104 |
| $\mu_{m,s}$ | $k_{s,s}$ | $\mu_{m,e}$ | $k_{s,e}$ | $\mu_{m,0}$ | $k_{s,0}$ |
| 3.5 | 0.1 | 0.17 | 0.1-0.5 | 0.256 | $0.1 \cdot 10^{-3}$ |

Table 3.1: Typical parameters values [73, 81]

$$\begin{aligned} \dot{x} &= (\mu_x - \lambda x)x \\ \dot{s} &= -\mu_s x + \lambda(s_i - s)x \\ \dot{e} &= (\mu_e - \lambda e)x \end{aligned} \tag{3.4}$$

## 3.3 Sliding mode existence and SMRC implementation

The control objective in this work is to control the biomass specific growth rate $\mu_x$ limiting, at the same time, the values of the ethanol flux. The block representation of the proposed control scheme, is provided in figure 3.2.

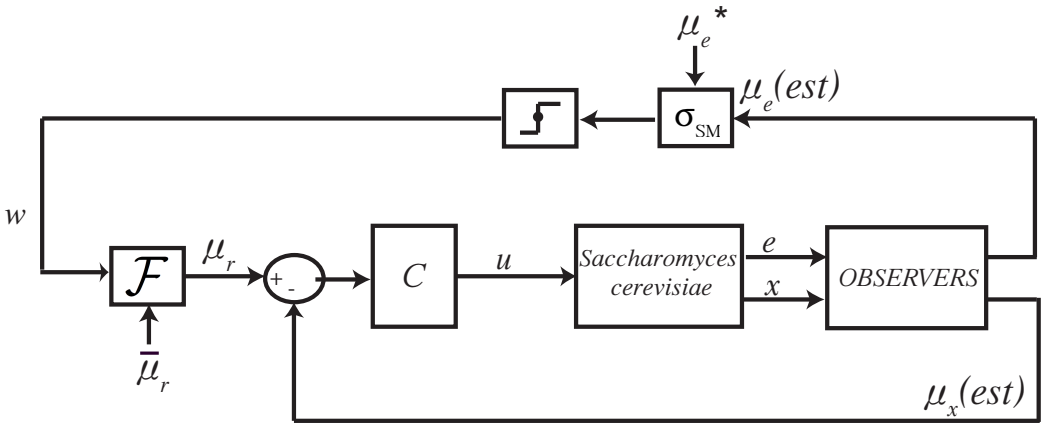


Figure 3.2: SMRC implementation for *Saccharomyces cerevisiae model*

As the SMRC loop is independent of the inner control loop, any of the controllers found in literature could be used as a inner loop controller with

the mission of leading $\mu_x$ to the desired reference. Here, it will be used the one proposed in [5]. Its expression is presented in 3.5.

$$\lambda = \lambda_r \left[1 - k(\mu_r - \hat{\mu}_x)\right] \tag{3.5}$$

where $\lambda_r$ and $k$ are constant gains, $\hat{\mu}_x$ is an estimation of the biomass specific growth rate and $\mu_r$ its desired reference value. The estimation $\hat{\mu}_x$ can be obtained using high gain observers from measurements of biomass [4].

The SMRC loop consists of a first order filter and a discontinuous block which is only active when the ethanol flux reaches the specified bound.

The filter expression takes the form:

$$F : \dot{\mu}_r = -\alpha(\mu_r + w - \bar{\mu}_r) \tag{3.6}$$

where $\mu_r$ is the conditioned reference, $\bar{\mu}_r$ is the desired reference when the SMRC is not active, $w$ is the discontinuous action and $\alpha$ a design parameter.

Combining equations 3.4, 3.5 and 3.6, and expressing them in a conventional form, the system takes the form:

$$\begin{bmatrix} \dot{x} \\ \dot{s} \\ \dot{\lambda} \\ \dot{e} \end{bmatrix} = \begin{bmatrix} \mu_x x - \lambda x^2 \\ -\mu_s x + \lambda(s_i - s)x \\ \lambda_r k \alpha \mu_r \\ (\mu_e - \lambda e)x \end{bmatrix} + \begin{bmatrix} 0 \\ 0 \\ \lambda_r k \alpha \\ 0 \end{bmatrix} w + \begin{bmatrix} 0 \\ 0 \\ \lambda_r k(\dot{\hat{\mu}}_x - \alpha \bar{\mu}_r) \\ 0 \end{bmatrix} \tag{3.7}$$

with $y_1 = \mu_x$ and $y_2$ defined, due to technical issues as $y_2 = \mu_e - \lambda e$

Note that the way $y_2$ is defined, helps in the subsequent calculations,

because with this definition, the relative degree from $y_2$ to the discontinuous signal $w$ is $gr = 1$. With $y_2 = \mu_e$ the relative degree would be $gr = 2$, forcing the inclusion of the first $y_2$ derivative in the sliding surface $\sigma$.

So, $\sigma$ can be defined as:

$$\sigma{=}(\mu_e{-}\lambda e){-}\bar{y}_2 \tag{3.8}$$

being the switching logic:

$$w{=}\left\{ \begin{array}{l} w^+ \; if \; \sigma{>}0 \\ 0 \; otherwise \end{array} \right\} \tag{3.9}$$

From 1.3.2, the existence condition that must be fulfilled so as the sliding mode to exist, is the trasversality condition, that is $L_g\sigma = \frac{\partial \sigma}{\partial x} g \neq 0$.

Equation 3.1 reveals that $\mu_e = \gamma_4 r_2 - r_3$ with $r_2$ and $r_3$ depending on $s$ and $e$ (see equations 3.2 and 3.3). $r_2$ regulates ethanol production whereas $r_3$ represents the rate at which ethanol is oxidized. These reactions can never occur at the same time, so, when $\mu_e$ is higher than 0, and ethanol is being produced, $r_3 = 0$ and $\mu_e{=}\gamma_4 r_2{=}\gamma_4(\mu_{m,s}\frac{s}{k_{s,s}+s}{-}(\gamma_5)^{-1}\mu_{m,o}\frac{o}{k_{s,o}+o})$.

In this way,

$$\frac{\partial \sigma}{\partial \mathrm{x}}{=}\left( \begin{array}{cccc} 0 & \mu_{m,s}\frac{k_{s,s}}{(k_{s,s}+s)^2} & -e & -\lambda \end{array} \right) \tag{3.10}$$

and

$$L_g\sigma=\frac{\partial\sigma}{\partial x}g=\begin{pmatrix} 0 & \mu_{m,s}\frac{k_{s,s}}{(k_{s,s}+s)^2} & -e & -\lambda \end{pmatrix}\begin{pmatrix} 0 \\ 0 \\ \lambda_r k\alpha \\ 0 \end{pmatrix}=-e\lambda_r k\alpha \qquad (3.11)$$

Note that the transversality condition is only fulfilled if the ethanol concentration is different from 0. Fortunately, that is the case when the sliding mode will be active.

In order to follow the invariance condition stated in 1.3.2 and, noting that in this case $L_g\sigma_1 < 0$, $w$ must be chosen to fit equation:

$$w\geq w^\sigma=-\frac{L_f\sigma}{L_g\sigma} \qquad (3.12)$$

with,

$$w^\sigma=-(\mu_{m,s}\frac{k_{s,s}}{(k_{s,s}+s)^2}(-\mu_s x+\lambda(s_i-s)x)-e\lambda_r k\alpha\mu_r-\lambda(\mu_e-\lambda e)x) \qquad (3.13)$$

As the process is controlled, all the variables are upper bounded so choosing, properly $\alpha$ and $w$ equation 3.12 can be fulfilled.

Remark that $\mu_e$ can not be measured, it has to be estimated. This estimation is carried out using Bastin observer[4] from ethanol measures, similarly to $\mu_x$ estimation.

## 3.4 Simulations

In order to test the efficiency of the proposed methodology, the model stated in 3.1 is simulated in a closed loop using 3.13 as a controller. Then, a sudden perturbation consisting of a temporal limitation in oxygen is considered. Looking at equation 3.2, it can be noticed that this perturbation activates $r_2$ and the subsequent ethanol production. It is in this moment when the SMRC loop becomes active, to limit the ethanol flux (in this case the expression $\mu_e - \lambda e$). Initial conditions are set to: biomass $x(0) = 0.5$, substrate $s(0) = 0.01$, ethanol $e(0) = 0$, volume $v(0) = 1$, and substrate concentration in the inlet flow $s_i = 20$.

The reference for the biomass specific growth rate when ethanol flux does not reach its upper bound ($\bar{\mu}_r$) is set to 0.25. The oxygen concentration is set to 0.4 mg/L, and at a given moment temporarily drops to 0.1 mg/L. $y_2$ ($\mu_e - \lambda e$) is limited to 0.02.

Figure 3.3, shows how, under a temporally limitation of oxygen, ethanol begins to be produced and if the ethanol flux (or the ethanol concentration) is not limited, the effect in the biomass rate $\mu_x$ is very high suffering an important drop. The constraints imposed in $y_2$, allows higher levels of $\mu_x$ even when substrate is in excess.

In figure 3.4, where the trajectories of the two terms of $y_2$ are plotted it can be appreciated how it does not exit the defined surface when the lack of oxygen takes part.

## 3.5 Discussion and future work

The work developed in this chapter has helped a lot in the design of future steps in this research line. It has been the first attemp to face the problem of

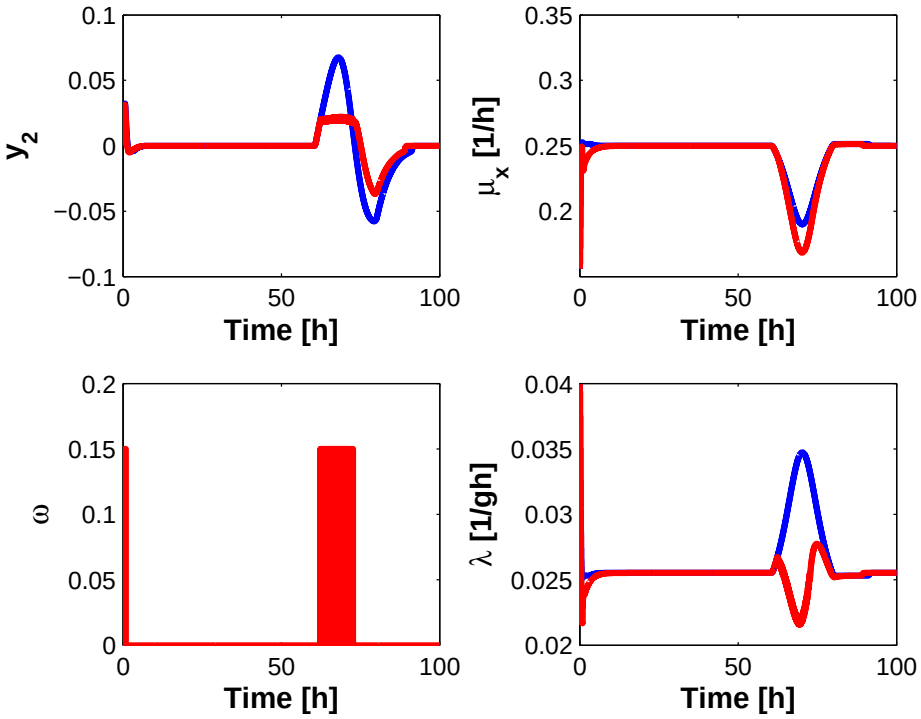


Figure 3.3: Sliding function, discontinuous function, biomass concentration rate and control action with (in red) and without (in blue) sliding mode reference conditioning.

controlling metabolic fluxes. In this case, the flux controlled was an external flux, but the idea is to extend this methodology to less accessible internal fluxes.

The first specific issue that will be found in this extension is that, depending on the flux to be controlled, it is possible that the relative degree from the flux to the discontinuous signal is greater than one. That fact, apart from complicating the mathematical demonstrations, forces to include in the sliding surface the first derivative of the flux to be controlled. An estimation of this derivative can be obtained using, for instance, Levant differentiators [44] adding an unavoidable noise to the system. This is the reason why in this work $y_2$ has been defined as $\mu_e - e\lambda$. Additionally, usually, neither

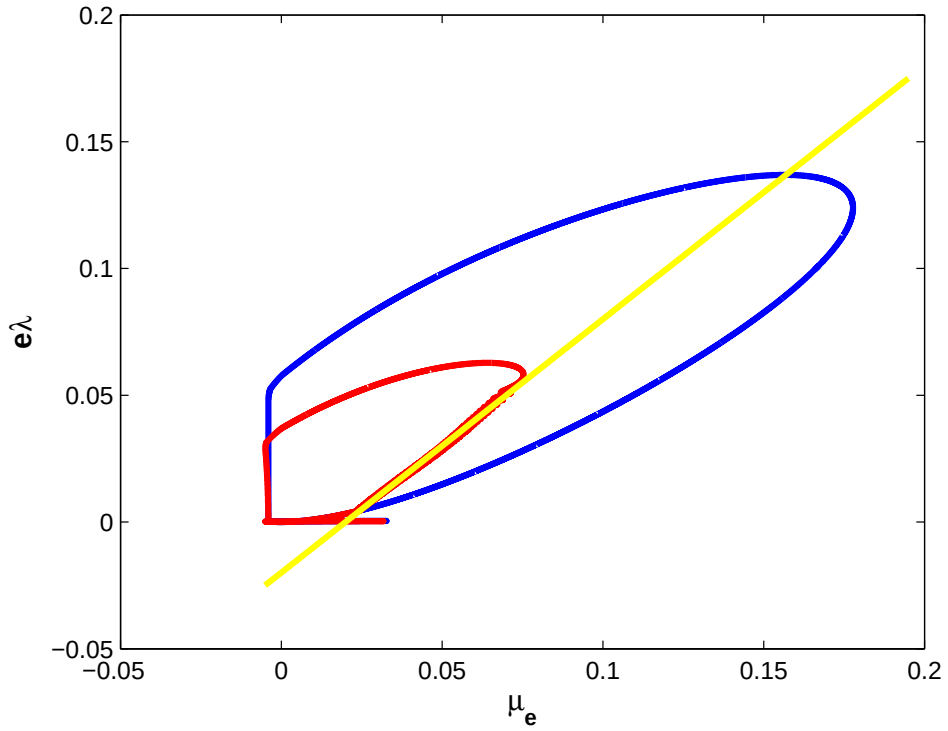


Figure 3.4: $\mu_e$ and $e\lambda$ trajectories on phase plane with the SMRC loop (red) and without it (blue). The yellow line represents the $y_2$ upper bound. Remember $y_2 = \mu_e - e\lambda$

the internal flux nor the concentrations of the internal metabolites can be measured, so they have to be estimated from measures of the external ones.

This estimation can be carried out using dynamic versions of the traditional metabolic flux analysis [82, 75, 26]. But, a more realistic scenario imposes the use of techniques capable of estimating those fluxes under uncertainty in the measures. In particular, interval and possibilistic MFA methods developed by Llaneras et al [46, 47] can be used to face (i) the uncertainty in the process and measurements, and (ii) the low ratio between measured variables versus model variables. The way the SMRC works under interval and possibilistic estimation of the fluxes is the second issue that must be studied in detail in future work.

Chapter 4

# Conclusions and future work

In this chapter, the achievements of this Master thesis will be reviewed, and a list of future items of pending work will be discussed.

Several tools for dealing with control subject to constraints in the area of biosystems have been explored in this work. The details of these tools are given in chapter 1. Then, the techniques are successfully applied to two different biosystems.

First, glucose control in diabetes type 1 mellitus is tackled in two ways. On one hand SIVIA algorithm is applied to obtain the set of basal-bolus combinations that will lead a good postprandial glucose control, fulfilling the constraints imposed by the IDF (non-hypoglycaemia and two-hour postprandial glucose value below 140 mg/dL). On the other hand and additional security SRMC loop is added to a glucose closed loop scheme so as to reduce the hypoglycaemia risk imposing some constraints in the IOB. Both approaches are proof of concept studies that may prelude the development of new robust nonempiric (CGM-based) tools, and more secure glucose closed loop systems respectively, aiding patients and physicians to attain a better metabolic control. This diabetes application was explained in chapter 2.

In chapter 3 an early attempt to the control of intracellular fluxes by

external actuation (*e.g.* substrate feeding rates) is presented. There, SRMC is used to optimize biomass production in *Saccharomyces cerevisiae* subject to constraints in ethanol flux. The potentiality of this approach and the difficulties that could be found in its internal flux extension are analized.

Note, that in both SRMc implementations (diabetes and ethanol applications) the features of the SM itself are inherited, but not the usual problems of SM like chattering and others, because the technique is going to be part of a numeric algorithm in a digital environment, and no discontinuous signals are actually applied to the processes.

## 4.1 Future work

This Master thesis has motivated many future work taking advance of the possibilities that the techniques studied here present. Moreover, the fact that the work developed here is framed in the context of two larger research projects, INSULAID2[1] and MULTISYSBIO[2], helps in encouraging the collaboration and increases the possibilities of future work.

In that way, parallel work is being developed by Alejandro Laguna [39, 40] to improve the most critical part of the **SIVIA algorithm** presented here, patients' identification following an OED. Clinical trials to evaluate the efficacy of the SIVIA based algorithm presented here *in vivo* using a clinical protocol for patients' identification are ongoing. Preliminary results will be presented in [69].Those experiments may help also to develop the most appropriate strategies for basal bolus selection, from all the feasible solutions.

On the other hand, some work is also been done by the research group so

[1] DPI2007-66728-C02-01 and DPI2007-66728-C02-02
[2] DPI2008-06880-C03-01, DPI2008-06880-C03-02 and DPI2008-06880-C03-03

as to reduce the computational cost of the algorithm, a necessary step before its implementation in future smart insulin pumps.

When talking about the **SMRC implementation to avoid hypoglycaemia**, many possibilities arose. The most evident one is the improvement of the feed-forward controller used here, in order to prevent as much as possible the delay in the control action. One possibility could be the combination of the two tools presented here, using SIVIA algorithm as feed-forward controller (see figure 2.18).

Moreover, this proposal could be also used, changing the way the problem is being seen, to help in the secure automatic tuning of controllers. The longer the time the SMRC loop is active, the higher is the hypoglycaemic risk without SRMC loop. In that way the controller parameters can be automatically regulated according to this strategy. This new potential use of the tool must be studied more deeply.

Finally, several future work actions can be derived from the **application of SRMC to limit ethanol flux** in *Saccharomyces cerevisiae*. First of all, this technique can be adapted to perform the control of less accessible internal fluxes. Since the intracellular fluxes have to be estimated and they will take the form of intervals or possibilistic distribution[46, 47], the control goal cannot be stated in terms of regulating to a single value. On the contrary, the objective will be to limit fluxes values to a certain regions, so that for the most possible situations, the regions are more restrictive whereas for the rest of situations, the restrictions can be relaxed.

The results of the extension of SMRC to the possibilistic frame can be tested using the model developed by the group of *Pichia Pastoris*[77] and CHO cells [63].

The final objective of future actions related to this work, will be to continue developing tools and extending the existing ones to deal with uncertainty in problems of control of processes subject to constraints in the

field of biosystems. In fact, uncertainty is one of the big problems that arise when working with this kind of systems.

# References


[1] M. Åkesson, P. Hagander, and J. Axelsson. A probing feeding strategy for Escherichia coli cultures. *Biotechnology techniques*, 13(8):523–528, 1999.

[2] G. Alefeld and J. Herzberger. *Interval analysis*. Academic Press, 1983.

[3] H. Amann. *Ordinary differential equations: an introduction to nonlinear analysis*. Walter de Gruyter, 1990.

[4] G. Bastin and D. Dochain. On-line estimation of microbial specific growth rates* 1. *Automatica*, 22(6):705–709, 1986.

[5] H. D. Battista, J.Picó, and E. Picó-Marco. Globally stabilizing control of fed-batch processes with Haldane kinetics using growth rate estimation feedback. *Journal of Process Control*, 16:865–875, 2006.

[6] J. Bondia, E. Dassau, H. Zisser, R. Calm, J. Vehí, L. Jovanovic, and F. J. Doyle III. Coordinated basal-bolus infusion for tighter postprandial glucose control in insulin pump therapy. *Journal of Diabetes Science and Technology*, 3(1):89–97, 2009.

[7] M. Brownlee. The pathobiology of diabetic complications. *Diabetes*, 54(6):1615–1625, June 2005.

[8] D. Bruttomesso, A. Farret, S. Costa, M. C. Marescotti, M. Vettore, A. Avogaro, A. Tiengo, C. D. Man, J. Place, A. Facchinetti, S. Guerra, L. Magni, G. D. Nicolao, C. Cobelli, E. Renard, and A. Maran. Closed-loop artificial pancreas using subcutaneous glucose sensing and insulin delivery and a model predictive control algorithm: preliminary studies in padova and montpellier. *Journal of Diabetes Science and Technology*, 3(5):1014–1021, 2009. PMID: 20144414.

[9] D. Campos-Delgado, M. Hernandez-Ordonez, R. Femat, and A. Gordillo-Moscoso. Fuzzy-based controller for glucose regulation in type-1 diabetic patients by subcutaneous route. *Biomedical Engineering, IEEE Transactions on*, 53(11):2201–2210, 2006.

[10] A. Caumo, R. Bergman, and C. Cobelli. Insulin sensitivity from meal tolerance tests in normal subjects: a minimal model index. *Journal of Clinical Endocrinology & Metabolism*, 85(11):4396, 2000.

[11] C. Chen and S. Peng. Design of a sliding mode control system for chemical processes. *Journal of Process Control*, 15:515–530, 2005.

[12] W. L. Clarke, S. Anderson, M. Breton, S. Patek, L. Kashmer, and B. Kovatchev. Closed-loop artificial pancreas using subcutaneous glucose sensing and insulin delivery and a model predictive control algorithm: the virginia experience. *Journal of Diabetes Science and Technology*, 3(5):1031–1038, 2009. PMID: 20144416.

[13] C. Cooney, H. Wang, and D. Wang. Computer-aided material balancing for prediction of fermentation parameters. *Biotechnology and bioengineering*, 19(1):55–67, 1977.

[14] M. A. Creager, T. F. Luscher, F. Cosentino, and J. A. Beckman. Diabetes and vascular disease: Pathophysiology, clinical consequences, and medical therapy: Part i. *Circulation*, 108(12):1527–1532, Sept. 2003.

[15] Diabetes Control and Complications Trial Research Group. The effect of intensive treatment of diabetes on the development and progression

of long-term complications in insulin-dependent diabetes mellitus. *The New England Journal of Medicine*, 329:977–986, 1993.

[16] C. Edwards, E. Fossas, and L. Fridman, editors. *Advances in Variable Structure and Sliding Mode Control*. Lecture Notes in Control and Information Sciences. Springer Berlin Heidelberg New York, 2006.

[17] C. Edwards and S. K. Spurgeon. *Sliding Mode Control: Theory and Applications*. Taylor & Francis, UK, 1st edition, 1998.

[18] D. Elleri, J. M. Allen, M. E. Wilinska, M. Nodale, J. S. Mangat, A. M. F. Larsen, C. L. Acerini, D. B. Dunger, and R. Hovorka. Fully automated overnight Closed-Loop glucose control in young children with type 1 diabetes. *Ninth Diabetes Technology Meeting*, A30, 2009.

[19] C. Ellingsen, E. Dassau, H. Zisser, B. Grosman, M. Percival, L. Jovanovič, and F. Doyle III. Safety constraints in an artificial pancreatic $\beta$ cell: An implementation of model predictive control with insulin on board. *Journal of diabetes science and technology (Online)*, 3(3):536, 2009.

[20] M. García-Jaramillo, R. Calm, J. Bondia, C. Tarín, and J. Vehí. Computing the risk of postprandial hypo- and hyperglycemia in. type 1 diabetes mellitus considering intrapatient variability and other sources of uncertainty. *Journal of Diabetes Science and Technology*, 3(4):895–902, 2009.

[21] W. Garcia-Gabin, J. Vehi, J. Bondia, C. Tarin, and R. Calm. Robust sliding mode closed-loop glucose control with meal compensation in type 1 diabetes mellitus. In *IFAC World Congress, 17th, Seoul*, 2008.

[22] F. Garelli, R. Mantz, and H. De Battista. Partial decoupling of non-minimum phase processes with bounds on the remaining coupling. *Chemical Engineering Science*, 61(23):7706–7716, 2006.

[23] P. Gresele, G. Guglielmini, M. D. Angelis, S. Ciferri, M. Ciofetta, E. Falcinelli, C. Lalli, G. Ciabattoni, G. Davi, and G. B. Bolli.

Acute, short-term hyperglycemia enhances shear stress-induced platelet activation in patients with type II diabetes mellitus. *J Am Coll Cardiol*, 41(6):1013–1020, Mar. 2003.

[24] R. Hanus, M. Kinnaert, and J. Henrotte. Conditioning technique, a general anti-windup and bumpless transfer method. *Automatica*, 23(6):729–739, 1987.

[25] L. Heinemann. Insulin pump therapy: What is the evidence for using different types of boluses for coverage of prandial insulin requirements? *Journal of Diabetes Science and Technology*, 3(6):1490–1500, 2009.

[26] O. Henry, A. Kamen, and M. Perrier. Monitoring the physiological state of mammalian cell perfusion processes by on-line estimation of intracellular fluxes. *Journal of Process control*, 17(3):241–251, 2007.

[27] G. Herrmann, S. Spurgeon, and C. Edwards. A model-based sliding mode control methodology applied to the HDA-plant. *Journal of Process Control*, 13(2):129–138, 2003.

[28] I. B. Hirsch. Insulin analogues. *N Engl J Med*, 352(2):174–183, Jan. 2005.

[29] R. Hovorka. The future of continuous glucose monitoring: closed loop. *Current Diabetes Reviews*, 4(3):269–279, Aug. 2008. PMID: 18690909.

[30] R. Hovorka, J. M. Allen, D. Elleri, L. J. Chassin, J. Harris, D. Xing, C. Kollman, T. Hovorka, A. M. F. Larsen, and M. Nodale. Manual closed-loop insulin delivery in children and adolescents with type 1 diabetes: a phase 2 randomised crossover trial. *The Lancet*, 375(9716):743–751, 2010.

[31] R. Hovorka, V. Canonico, L. J. Chassin, U. Haueter, M. Massi-Benedetti, M. O. Federici, T. R. Pieber, H. C. Schaller, L. Schaupp, T. Vering, and M. E. Wilinska. Nonlinear model predictive control of glucose concentration in subjects with type 1 diabetes. *Physiol Meas*, 25(4):905–920, 2004.

[32] R. Hovorka, F. Shojaee-Moradie, P. V. Carroll, L. J. Chassin, I. J. Gowrie, N. C. Jackson, R. S. Tudor, A. M. Umpleby, and R. H. Jones. Partitioning glucose distribution/transport, disposal, and endogenous production during IVGTT. *Am J Physiol Endocrinol Metab*, 282(5):E992–1007, May 2002.

[33] J. Hung, W. Gao, and J. Hung. Variable structure control: a survey. *IEEE Transactions on Industrial Electronics*, 40(1):2–22, 1993.

[34] L. Hung, H. Lin, and H. Chung. Design of self-tuning fuzzy sliding mode control for TORA system. *Expert Systems with Applications*, 32(4):1164–1182, 2007.

[35] M. Ibbini and M. Masadeh. A fuzzy logic based closed-loop control system for blood glucose level regulation in diabetics. *Journal of Medical Engineering & Technology*, 29(2):64–69, 2005.

[36] International Diabetes Federation. Guideline for management of postmeal glucose.

[37] B. P. Kovatchev, M. Breton, C. Dalla Man, and C. Cobelli. In silico preclinical trials: A proof of concept in closed-loop control of type 1 diabetes. *Journal of Diabetes Science and Technology*, 3(1):44–55, 2009.

[38] L. Jaulin, M. Kieffer, O. Didrit, and E. Walter. *Applied Interval Analysis*. Springer, 2001.

[39] A. J. Laguna, P. Rossetti, F. J. Ampudia-Blasco, J. Vehí, and J. Bondia. Improving postprandial model identification using ambulatory data from type 1 diabetic patients. In *10th annual Diabetes Technology Meeting*, 2010.

[40] A. J. Laguna, P. Rossetti, F. J. Ampudia-Blasco, J. Vehí, and J. Bondia. Optimal design for individual model identification based on ambulatory continuous glucose monitoring in patients with type 1 diabetes. In *UKACC International Conference on Control 2010*, 2010.

[41] A. Laguna Sanz. Model identification from ambulatory data for post-prandial glucose control in type 1 diabetes. Master's thesis, Universidad Politécnica de Valencia, 2010.

[42] N. Lai, C. Edwards, and S. Spurgeon. An implementation of an output tracking dynamic discrete-time sliding mode controller on an aircraft simulator. In *Proceedings of the 2006 International Workshop on Variable Structure Systems, VSS'06*, pages 35–40. IEEE-CSS, 2006.

[43] E. Lehmann, C. Tarín, J. Bondia, E. Teufel, and T. Deutsch. Incorporating a Generic Model of Subcutaneous Insulin Absorption into the AIDA v4 Diabetes Simulator: 1. A Prospective Collaborative Development Plan. *Journal of diabetes science and technology (Online)*, 1(3):423, 2007.

[44] A. Levant. Higher-order sliding modes, differentiation and output-feedback control. *International Journal of Control, 76*, 9(10):924–941, 2003.

[45] L. Ljung. *System Identification: Theory for the User (2nd Edition)*. Prentice Hall PTR, December 1999.

[46] F. Llaneras and J. Picó. A procedure for the estimation over time of metabolic fluxes in scenarios where measurements are uncertain and/or insufficient. *BMC bioinformatics*, 8(1):421, 2007.

[47] F. Llaneras, A. Sala, and J. Picó. A possibilistic framework for constraint-based metabolic flux analysis. *BMC Systems Biology*, 3(1):79, 2009.

[48] L. Magni, D. M. Raimondo, L. Bossi, C. D. Man, G. D. Nicolao, B. Kovatchev, and C. Cobelli. Model predictive control of type 1 diabetes: an in silico trial. *Journal of Diabetes Science and Technology*, 1(6):804?812, 2007.

[49] C. Man, M. Camilleri, and C. Cobelli. A system model of oral glucose absorption: validation on gold standard data. *Biomedical Engineering, IEEE Transactions on*, 53(12):2472–2478, 2006.

[50] C. D. Man, R. A. Rizza, and C. Cobelli. Meal simulation model of the glucose-insulin system. *IEEE Transactions on Bio-Medical Engineering*, 54(10):1740–1749, Oct. 2007. PMID: 17926672.

[51] R. Mantz and H. De Battista. Sliding Mode Compensation for Windup and Direction of Control Problems in Two-Input- Two-Output Proportional- Integral Controllers. *Ind. Eng. Chem. Res*, 41(13):3179–3185, 2002.

[52] R. Mantz, H. De Battista, and F. Bianchi. Sliding mode conditioning for constrained processes. *Ind. Eng. Chem. Res*, 43(26):8251–8256, 2004.

[53] G. Marchetti, M. Barolo, L. Jovanovic, H. Zisser, and D. Seborg. An improved PID switching control strategy for type 1 diabetes. *Biomedical Engineering, IEEE Transactions on*, 55(3):857–865, 2008.

[54] J. Mareczek, M. Buss, and M. Spong. Invariance control for a class of cascade nonlinear systems. *Automatic Control, IEEE Transactions on*, 47(4):636–640, 2002.

[55] L. Monnier, C. Colette, G. J. Dunseath, and D. R. Owens. The loss of postprandial glycemic control precedes stepwise deterioration of fasting with worsening diabetes. *Diabetes Care*, 30(2):263–269, Feb. 2007.

[56] R. E. Moore. *Interval analysis*. Prentice-Hall Inc., Englewood Cliffs, N.J., 1966.

[57] J. Nielsen, J. Villadsen, and G. Lidén. *Bioreaction engineering principles*. Plenum Pub Corp, 2003.

[58] D. Office of Technology Assessment, Washington. Commercial biotechnology: An international analysis. Technical report, Office of Technology Assessment, Washington, DC, 1984.

[59] N. Oliver, P. Georgiou, D. Johnston, and C. Toumazou. A Benchtop Closed-loop System Controlled by a Bio-Inspired Silicon Implementation of the Pancreatic beta Cell. *Journal of diabetes science and technology*, 3(6):1419, 2009.

[60] R. Parker, F. Doyle III, J. Ward, and N. Peppas. Robust H? glucose control in diabetes using a physiological model. *AIChE Journal*, 46(12):2537–2549, 2000.

[61] W. Perruquetti and J. P. Barbot, editors. *Sliding Mode Control in Engineering*. Control Engineering Series. Marcel Dekker, 2002.

[62] J. Picó, F. Garelli, H. De Battista, and R. Mantz. Geometric invariance and reference conditioning ideas for control of overflow metabolism. *Journal of Process Control*, 19(10):1617–1626, 2009.

[63] A. Provost, G. Bastin, S. Agathos, and Y. Schneider. Metabolic design of macroscopic bioreaction models: application to Chinese hamster ovary cells. *Bioprocess and biosystems engineering*, 29(5):349–366, 2006.

[64] G. Quiroz and R. Femat. Theoretical blood glucose control in hyper- and hypoglycemic and exercise scenarios by means of an H [infinity] algorithm. *Journal of theoretical biology*, 263(1):154–160, 2010.

[65] R. E. Moore. *Methods and Applications of Interval Analysis*. SIAM Studies in Applied and Numerical Mathematics, 1979.

[66] P. C. Ratledge and B. Kristiansen. *Basic Biotechnology*. Cambridge University Press, 2nd, illustrated, revised edition, 2001.

[67] A. Revert, R. Calm, J. Vehi, and J. Bondia. Calculation of the best basal-bolus combination for postprandial glucose control in insulin pump therapy. *Biomedical Engineering, IEEE Transactions on*, 58(2):274 – 281, 2011.

[68] A. Revert, P. Rossetti, R. Calm, J. Vehí, and J. Bondia. Combining Basal bolus insulin infusion for tight postprandial glucose control: an in

silico evaluation in adults, children, and adolescents. *Journal of diabetes science and technology*, 4(6):1424, 2010.

[69] P. Rosseti, F. Ampudia-Blasco, A. Laguna, A. Revert, J. Vehi, R. Calm, S. Correa, G. Viguer, J. Ascaso, and J. Bondia. Calculo del bolus prandial utilizando monitorización continua de la glucosa en pacientes con diabetes mellitus tipo 1 tratados con infusión subcutánea de insulina. In *XXII Congreso Nacional de la Sociedad Española de Diabetes*, 2011.

[70] E. Ruiz-Velazquez, R. Femat, and D. Campos-Delgado. Blood glucose control for type I diabetes mellitus: A robust tracking H [infinity] problem. *Control Engineering Practice*, 12(9):1179–1195, 2004.

[71] H. Sira-Ramírez. Differential geometric methods in variable structure systems. *International Journal of Control*, 48(4):1359–1390, 1988.

[72] H. Sira-Ramírez. Sliding regimes in general non-linear systems: a relative degree approach. *International Journal of Control*, 50:1487–1506, 1989.

[73] B. Sonnleitner and O. Käpeli. Growth of *Saccharomyces cerevisiae* is controlled by its limited respiratory capacity: formulation and verification of a hypothesis. *Biotechnology and Bioengineering*, 28:927–937, 1986.

[74] G. M. Steil, K. Rebrin, C. Darwin, F. Hariri, and M. F. Saad. Feasibility of automating insulin delivery for the treatment of type 1 diabetes. *Diabetes*, 55(12):3344–3350, Dec. 2006.

[75] G. Stephanopoulos, A. Aristidou, J. Nielsen, and J. Nielsen. *Metabolic engineering: principles and methodologies*. Academic Pr, 1998.

[76] D. Takahashi, Y. Xiao, and F. Hu. A survey of insulin-dependent diabetes-part II: control methods. *International Journal of Telemedicine and Applications*, 2008:1–14, 2008.

[77] M. Tortajada, F. Llaneras, and J. Picó. Validation of a constraint-based model of Pichia pastoris metabolism under data scarcity. *BMC Systems Biology*, 4(1):115, 2010.

[78] UK Prospective Diabetes Study (UKPDS) Group. Intensive blood-glucose control with sulphonylureas or insulin compared with conventional treatment and risk of complications in patients with type 2 diabetes (UKPDS 33). *Lancet*, 352(9131):837–853, Sept. 1998. PMID: 9742976.

[79] V. Utkin. Variable structure systems with sliding modes. *IEEE Transactions on Automatic Control*, 22(2):212–222, 1977.

[80] V. Utkin, J. Guldner, and J. Shi. *Sliding Mode Control in Electromechanical Systems*. Taylor & Francis, London, 1st edition, 1999.

[81] S. Valentinotti, B. Srinivasan, U. Holmberg, D. Bonvin, C. Cannizzaro, M. Rhiel, and U. von Stockar. Optimal operation of fed-batch fermentations via adaptive control of overflow metabolite. *Control Engineering Practice*, 11:665–674, 2003.

[82] R. Van der Heijden, J. Heijnen, C. Hellinga, B. Romein, and K. Luyben. Linear constraint relations in biochemical reaction systems: I. Classification of the calculability and the balanceability of conversion rates. *Biotechnology and bioengineering*, 43(1):3–10, 1994.

[83] W. Waldhäusl. Circadian rhythms of insulin needs and actions. *Diabetes Research and Clinical Practice*, 6(4):S17–S24, 1989.

[84] K. Walgama, S. Rönnbäck, and J. Sternby. Generalization of conditioning technique for anti-windup compensators. *IEE Proceedings on Control Theory and Applications*, 139(2):109–118, March 1992.

[85] J. Walsh. Changes in diabetes care: a history of insulin and pumps past, present, and future., 2004.

[86] J. Walsh and R. Roberts. *Pumping insulin: everything you need for success on a smart insulin pump*. Torrey Pines Pr, 2006.

[87] E. Walter and L. Pronzato. *Identification of parametric models from experimental data.* Communications and Control Engineering Series. Berlin: Springer. xviii, 413 p., 1997.

[88] S. A. Weinzimer, G. M. Steil, K. L. Swan, J. Dziura, N. Kurtz, and W. V. Tamborlane. Fully automated Closed-Loop insulin delivery versus semiautomated hybrid control in pediatric patients with type 1 diabetes using an artificial pancreas. *Diabetes Care*, 31(5):934–939, 2008.

[89] M. Wilinska, L. Chassin, C. Acerini, J. Allen, D. Dunger, and R. Hovorka. Simulation Environment to Evaluate Closed-Loop Insulin Delivery Systems in Type 1 Diabetes. *Journal of diabetes science and technology*, 4(1):132, 2010.

[90] K. Young, V. Utkin, and U. Ozgüner. A control engineer's guide to sliding mode control. *IEEE Transactions on Control Systems Technology*, 7(3):328–342, 1999.

[91] F. Zaccardi, D. Pitocco, and G. Ghirlanda. Glycemic risk factors of diabetic vascular complications: the role of glycemic variability. *Diabetes/Metabolism Research and Reviews*, 25(3):199–207, Mar. 2009. PMID: 19172575.

[92] Y. Zheng, H. Kreuwel, D. Young, L. Shoda, S. Ramanujan, K. Gadkar, M. Atkinson, and C. Whiting. The Virtual NOD Mouse. *Annals-New York Academy of Sciences*, 1103:45, 2007.

[93] H. Zisser, L. Robinson, W. Bevier, E. Dassau, C. Ellingsen, F. J. Doyle, and L. Jovanovic. Bolus calculator: A review of four "smart" insulin pumps. *Diabetes Technology & Therapeutics*, 10(6):441–444, 2008.